



# 1 Measurement of alkyl and multifunctional organic nitrates 2 by Proton Transfer Reaction Mass Spectrometry

3

4 **Marius Duncianu<sup>1</sup>, Marc David<sup>1</sup>, Sakthivel Kartigeyane<sup>1</sup>, Manuela Cirtog<sup>1</sup>,**  
5 **Jean-Francois Doussin<sup>1</sup>, and Benedicte Picquet-Varrault<sup>1</sup>**

6 [1] Laboratoire Interuniversitaire des Systèmes Atmosphériques (LISA), UMR-CNRS  
7 7583, Université Paris-Est-Créteil (UPEC) et Université Paris Diderot (UPD), France,

8 Correspondence to: benedicte.picquet-varrault@lisa.u-pec.fr

9

## 10 Highlights

- 11 • PTR-MS technique is proposed as a reliable measurement tool of individual organic  
12 nitrates.
- 13 • Different classes of organic nitrates are characterized from the mass spectrometric point  
14 of view.
- 15 • Different ionization modes and reagent ions are proposed for each type of organic  
16 nitrates.

17

## 18 Abstract

19 A commercial PTR-ToF-MS has been optimized in order to allow the measurement of  
20 individual organic nitrates in the atmosphere. This has been accomplished by shifting the  
21 distribution between different ionizing analytes,  $\text{H}_3\text{O}^+/\text{H}_3\text{O}^+(\text{H}_2\text{O})_n$  or  $\text{NO}^+/\text{NO}_2^+$ . The  
22 proposed approach has been proved to be appropriate for the on-line detection of individual  
23 alkyl nitrates and functionalized nitrates. It has been shown that hydroxyl- and keto-nitrates  
24 have a high affinity towards  $\text{NO}^+$ , leading to the formation of an adduct that allows to easily  
25 identify the organic nitrate (R) with the R- $\text{NO}^+$  ion signal. The recorded sensitivities for both  
26 ionization modes correspond to detection limits of tens of ppt  $\text{min}^{-1}$  in the case of hydroxy-  
27 and keto-nitrates. Alkyl nitrates exhibit a moderate affinity towards  $\text{NO}^+$  ionization leading to  
28 detection units of few hundreds of ppt and the highest sensitivity in  $\text{H}_3\text{O}^+$  mode was obtained  
29 for the water adducts signals. This method exhibits however lower capabilities for the  
30 detection of PANs with detection limits in the ppb range.



31

## 32 **1 Introduction**

33 Organic nitrates are important species of the reactive nitrogen (NO<sub>y</sub>) budget in the  
34 troposphere. They are formed in NO<sub>x</sub> rich air by the degradation of hydrocarbons initiated by  
35 OH (daytime) and NO<sub>3</sub> (nighttime) radicals. Since organic nitrates have lifetimes of several  
36 days or weeks (Perring et al., 2013), they can act as reservoirs for reactive nitrogen by  
37 undergoing long-range transport in the free troposphere before decomposing and releasing  
38 NO<sub>x</sub>. They play therefore a key role in the ozone formation as they sequester reactive  
39 nitrogen in rich NO<sub>x</sub> regions and release it in regions where production of ozone may be NO<sub>x</sub>  
40 limited. The significant impact of organic nitrates chemistry on ozone budget has been  
41 confirmed by recent modelling studies (Curci et al., 2009; Horowitz et al., 2007).

42 In addition, several field studies have shown that both polluted and remote atmospheres  
43 contain a large variety of organic nitrates which significantly affects the NO<sub>y</sub> budget (for  
44 example, 35 - 40 % as reported by Buhr et al. (1990) and up to 70% according to a modeling  
45 study performed by Madronich and Calvert (1990)). They are monofunctional alkyl nitrates,  
46 PANs but also multifunctional alkyl nitrates (Browne et al., 2013; Fischer et al., 2000; Kastler  
47 and Ballschmiter, 1999; Muthuramu et al., 1993; O'Brien et al., 1995). These latter include i)  
48 hydroxynitrates which are formed by the oxidation of alkenes initiated by OH radicals and by  
49 isomerisation processes of alkoxy radicals (Arey et al., 2001), ii) carbonyl-nitrates which are  
50 produced by the NO<sub>3</sub>-oxidation of alkenes but are also second-generation oxidation products  
51 of hydrocarbons and iii) dinitrates which are also expected to be second-generation oxidation  
52 products (Atkinson, 2000; Barnes et al., 1990; Roberts, 1990).

53 However, measurements of organic nitrates during field campaigns remain rare preventing a  
54 precise evaluation of their impact on the NO<sub>y</sub> budget in a wide variety of environments. The  
55 main problems in analyzing organic nitrates in the atmosphere are first the great complexity  
56 of the mixtures due to the huge number of precursors and formation pathways and then the  
57 fact that organic nitrates are explosive compounds and only few of them are commercial. So  
58 standards have to be synthesized. These analytical difficulties also affect our capability to  
59 study the chemical processes in which organic nitrates are involved during lab experiments  
60 (e.g. in simulation chambers).



61 Table 1 summarizes, without the intent of being exhaustive, some keystone articles  
62 concerning the organic nitrates analysis in field and laboratory studies.

63 Two approaches have been applied for the analysis of complex mixtures of organic nitrates  
64 during field and lab experiments: first, analyses at the molecular scale which is a powerful  
65 approach to elucidate mechanisms but has the drawback to be often limited to a low number  
66 of species and then, functional group analyses which are very useful to assess global budgets  
67 but bring poor information for the understanding of processes. The second approach allows to  
68 shortcut the complexity of the organic nitrates chemistry governing their production,  
69 transformation, and removal processes and assess directly the sum of peroxy nitrates  $\Sigma$ AN and  
70 alkyl nitrates  $\Sigma$ AN (Day et al., 2002; Perring et al., 2010). The thermal dissociation (TD)  
71 properties of different classes of nitrates was used as an analytical tool able to sketch the  
72 global chemistry of  $\text{RONO}_2$ , same as the Laser-Induced Florescence (LIF), cavity ring down  
73 spectroscopy (CRDS)(Paul et al., 2009), or cavity attenuated phase shift (CAPS)(Sadanaga et  
74 al., 2016), were used to quantify the  $\text{NO}_2$  issued from the organic nitrates decomposition. In a  
75 similar way, the infrared spectroscopy (IR) was used to monitor the time dependent loss of  
76 organic nitrates and measure the rate of homolytic O–N bond cleavage (Francisco and  
77 Kryłowski, 2005) employing specific absorption bands in IR ( $1638 \text{ cm}^{-1}$ ). Although  
78 notoriously powerful analytical techniques, the LIF, CRDS, CAPS and the IR exhibit poor  
79 capabilities in the individual quantification of organic nitrates mixtures due to their intrinsic  
80 conceptual operation mode.

81 Historically, measurements of individual organic nitrates have been conducted by gas  
82 chromatography coupled to electron capture detection - GC/ECD, both coupled or not (Atlas,  
83 1988; Blake et al., 1999; Flocke et al., 2005; Fukui and Doskey, 1998; Muthuramu et al.,  
84 1993), to a pyrolysis/luminol chemiluminescence - CL detector (Buhr et al., 1990; Fischer et  
85 al., 2000; Flocke et al., 1991; Gaffney et al., 1999; Hao et al., 1994; Winer et al., 1974), to  
86 electron impact mass spectrometry EI-MS (Luxenhofer and Ballschmiter, 1994; Luxenhofer  
87 et al., 1994) or to negative ion chemical ionization mass spectrometry – NI/CI-MS (Beaver et  
88 al., 2012; Tanimoto et al., 1999) using thermal electrons ( $e_{th}^-$ ). Abundant in marine  
89 environments, the halocarbons are highly sensitive towards the ECD detection (Fischer et al.,  
90 2002; Fischer et al., 2000) and may generate artifacts in the organic nitrates identification and  
91 quantification (Fukui and Doskey, 1998).



92 Although the chromatographic separation represents an effective analytical tool, the organic  
93 nitrates identification relies mainly on the retention times, while the dedicated detectors are  
94 only able to confirm, in best case, the presence of the nitrate functional group in the molecule.  
95 Illustrative examples are given by the studies of Luxenhofer et al. (1994) and Kastler and  
96 Ballschmiter (1999) who succeeded to analyze complex mixtures of alkyl and multifunctional  
97 organic nitrates by combining separation with liquid and gas chromatography and detection  
98 using the intense mass-to-charge ( $m/z$ ) 46 fragment ion that corresponds to  $\text{NO}_2^+$ . The same  
99 study highlights possible interferences with dinitrophenols, nitro- and dinitrocresols,  
100 pentachloro-nitrobenzene and to a smaller extent nitrophenols.

101 Besides the poor temporal resolution, another major drawback of this method is represented  
102 by the recovery factor decline with longer times in the chromatographic columns. According  
103 to Roberts et al. (2002), the sensitivity of this method for PANs is characterized by a  
104 diminishing response factor proportional to the compounds retention time through the  
105 column. Measurement of functionalized (oxygenated) nitrates appears to be a greater  
106 challenge as the lower vapor pressures and stronger surface interactions of these molecules  
107 make sampling and chromatographic techniques less appropriate. Additionally, the detection  
108 of functionalized nitrates by electron impact mass spectrometry has proven to be difficult,  
109 mainly due to the instability and thus, the fragmentation, of the molecular ion formed (Mills et  
110 al., 2016; Roberts, 1990; Rollins et al., 2010).

111 Lately, the newly developed capabilities in Atmospheric Pressure / Chemical Ionization Mass  
112 Spectrometry (AP-CIMS; CIMS) (Huey, 2007; Perraud et al., 2010; Slusher et al., 2004; Teng  
113 et al., 2014) prone as potentially powerful tools in organic nitrates analysis. Several types of  
114 CIMS have been highlighted by the literature, the technique being currently in progress.

115 The AP-CIMS uses methanol as a proton source in order to generate  $\text{RH}^+$  peaks of the parent  
116 ions. Therefore the nitrogen-containing ions are characterized by even  $m/z$  ratios, while the  
117 analytes containing only C, H, and O appear at odd  $m/z$ . Several PANs were identified as gas  
118 phase products of the  $\alpha$ -pinene +  $\text{NO}_3$  reaction with this technique (Perraud et al., 2010). The  
119 protonated molecular ions were identified and the most intense fragments in the MS/MS scan  
120 corresponds to losses of  $\text{NO}_2$ ,  $\text{HNO}_3$  and to a smaller extent  $\text{HOONO}_2$ . Hydroxynitrates and  
121 keto-nitrates have also been detected with this technique. For hydroxynitrates,  $\text{RH}^+$  peaks as  
122 well as fragments corresponding to the losses of  $\text{H}_2\text{O}$  and  $\text{NO}_2 + \text{H}_2\text{O}$  in the MS/MS mode  
123 were detected (Perraud et al., 2010; Schoon et al., 2007; Tuazon et al., 1999).



124 The thermal dissociation–chemical ionization mass spectrometry (TD-CIMS) technique has  
125 been used for measurement of PANs and other multifunctional organic nitrates by the means  
126 of I<sup>-</sup> reaction (Lee et al., 2014; Slusher et al., 2004; Xiong et al., 2015). The obtained  
127 carboxylate ion is unique for each parent species, and the only significant interference that has  
128 been identified is at ppb levels of NO (Slusher et al., 2004). The CF<sub>3</sub>O<sup>-</sup> was equally  
129 successfully tested as ionizing source in a CIMS approach in order to identify hydroxy-  
130 nitrates formed during the OH oxidation of alkenes in the presence of O<sub>2</sub> and NO (Bates et al.,  
131 2014; Teng et al., 2014). The quantification of the nitrates formed was assured by a  
132 complementary TD-LIF technique after subsequent GC separation. Other polyfunctional  
133 organic nitrates were scarcely detected using this technique.

134 The Proton-Transfer Reaction Mass Spectrometry (PTR-MS) can be positioned as a subset of  
135 CI. Its use in atmospheric research has expanded rapidly these last years but few studies have  
136 tested this technique for the detection of organic nitrates (Aoki et al., 2007; Hansel and  
137 Wisthaler, 2000; Inomata et al., 2013).

138 The recent study of Müller et al. (2012) considers that the quantification of PAN by PTR-MS  
139 is difficult due to fragmentation. Less promising results are also reported by Aoki et al. (2007)  
140 concerning the PTR ionization of C<sub>1</sub>–C<sub>5</sub> alkyl nitrates. Considerable fragmentation occurs,  
141 even at low field density (E/N) ratio (100 Td; *E* being the electric field strength and *N* the gas  
142 number density; 1 Td = 10<sup>-17</sup> V cm<sup>2</sup>), the signal intensities of protonated alkyl nitrates,  
143 (ROH·NO<sub>2</sub>)<sup>+</sup>, being in best case, a few percent of those of the total ion signals. An increase of  
144 the E/N ratio increases furthermore the fragmentation, providing common ions such as NO<sub>2</sub><sup>+</sup>  
145 and more characteristic ones such as RO<sup>+</sup>. Other low intensity signals corresponding to R<sup>+</sup> or  
146 ROH·H<sup>+</sup> ions have been also recorded and could result from reactions of alkyl nitrates with  
147 H<sub>3</sub>O<sup>+</sup>(H<sub>2</sub>O)<sub>n</sub> clusters.

148 Hansel and Wisthaler (2000) have measured several PANs (PAN, MPAN and PPN) with  
149 PTR-MS and have reported low detection limit (70 pptv, 15s integration time) and an overall  
150 accuracy of 15 %. Worth noticing that the reported analytical sensitivities (15-25 counts ppb<sup>-1</sup>)  
151 have not been calculated for the molecular ion signal but for typical molecular fragments in  
152 the case of the alkyl nitrates or signals of speculative subsequent reaction products of the  
153 protonated molecular ions for PANs. These results are illustrative for the organic nitrates  
154 overall affinity towards fragmentation due to chemical ionization in a low pressure drift tube



155 under high voltage. To our knowledge, polyfunctional organic nitrates have never been  
156 detected using this technique.

157 So, it appears useful to better explore the possibility of detecting organic nitrates in real-time  
158 with PTR-MS. In the present work, the detection of alkyl and multifunctional organic nitrates  
159 (PANs, ketonitrates, hydroxynitrates) by this technique was investigated. For this purpose,  
160 different organic nitrates were synthesized and mixtures at the ppb-ppm level were generated  
161 in a smog chamber. A commercial PTR-ToF-MS instrument was used but the operating mode  
162 as well as the chemical ionization reagent have been modified and optimized for each type of  
163 organic nitrate in order to gain sensibility in the detection and to reduce fragmentation of ions.  
164 Mass spectra have been carefully interpreted and detection limits have been also determined.

165

## 166 **2 Material and methods**

### 167 **2.1 Instrumentation**

168 A commercially available, high mass resolution PTR-ToF-MS instrument (Kore Technology -  
169 'Series II' High Performance PTR-TOF-MS) was used in the present study. The mass  
170 resolution of this instrument is  $>5000 M/\delta M$ . The PTR-MS is equipped with the newly  
171 designed radio frequency ion funnel (RF) which is used to focus ions in the drift tube and  
172 hence to increase the detection sensitivity (Barber et al., 2012). This ion funnel uses a series  
173 of electrodes with progressively reducing aperture sizes. In addition to the standard dc  
174 electrical field, an ac electric field is provided at a radio frequency creating a strongly  
175 repulsive effective potential near the surface of the electrodes, which combined to the  
176 reducing aperture sizes, serves to focus the ions radially. This system has been shown to  
177 increase the sensitivity by one or two orders of magnitude (Barber et al., 2012). Worth notice  
178 that operating in the RF mode modifies the dynamic range over which the drift tube is  
179 operated and the contribution of the radiofrequency to the global effective E/N ratio remains  
180 difficult to estimate (Barber et al., 2012).

181 The PTR-MS sampling line was designed in order to assure the highest transfer efficiency of  
182 the compounds. This line is made of a 1.5 meter long Silcosteel® coated stainless steel  
183 tubing, which has been shown to be appropriated for the transfer of low-level polar organic  
184 compounds (Smith, 2003). This line was heated at 40°C in order to prevent adsorption of



185 compounds in the line. With a sampling flow rate of  $\sim 3 \text{ cm}^3 \text{ s}^{-1}$ , the residence time in the line  
186 has been estimated to be lower than 2s. The PTR-MS inlet system is equally made with  
187 Silcosteel® coated stainless steel tubing and is equipped with a temperature control unit  
188 allowing heating up to 150°C.

## 189 2.2 Experimental strategy

190 In PTR-MS, proton transfer reactions with hydronium ions ( $\text{H}_3\text{O}^+$ ) are typically used to ionize  
191 compounds having a proton affinity (PA) higher than the one of water ( $691 \text{ kJ mol}^{-1}$ , Hunter  
192 and Lias, 1998):



194 In this case, the proton transfer reaction is exothermic and proceeds at a reaction rate close to  
195 the collision rate ( $10^{-9} \text{ cm}^3 \text{ molecule}^{-1} \text{ s}^{-1}$ ; Flocke et al. (1991)). In order to avoid a massive  
196 fragmentation of the analyte and consequently a decrease of the intensity and the specificity  
197 of the analytical signal, the energy transferred during the reaction should be lower than the  
198 bond energies of the compound of interest.

199 Only few available data can be found concerning the PA of organic nitrates which were  
200 calculated using *ab initio* quantum mechanical methods exclusively. The PA of organic  
201 nitrates have been estimated to:  $740 \text{ kJ mol}^{-1}$  for methyl nitrate (Lee and Rice, 1992),  $753 \text{ kJ}$   
202  $\text{mol}^{-1}$  for ethyl nitrate (Kriemler and Buttrill, 1970),  $748 \text{ kJ mol}^{-1}$  for methylperoxy nitrate  
203 (Ravelo and Francisco, 2007) and  $759\text{--}773 \text{ kJ mol}^{-1}$  for peroxyacetyl nitrate (Tureček, 2000).  
204 These studies show that the PA of organic nitrates are higher than the one of water and so that  
205 proton transfer reaction may occur. Furthermore, the functionalized nitrates concerned by the  
206 current study are equally expected to easily protonate as it was shown that the presence of an  
207 additional oxygen atom in the molecule enhances the overall PA (Ravelo and Francisco,  
208 2007).

209 It is well known that other chemical processes can also occur in the PTR reactor (Blake et al.,  
210 2009; de Gouw and Warneke, 2007). The  $\text{H}_3\text{O}^+$  and  $\text{R}^+$  can cluster with water molecules in  
211 the sampled air. The water cluster ions formation in the PTR cell is generally considered as  
212 problematic since their presence complicates the mass spectra treatment. Typically, their  
213 formation is limited by high kinetic energy of the ions into the drift tube at E/N ratios superior  
214 to 100 Td. However, the proton-transfer reaction of  $\text{H}_3\text{O}^+(\text{H}_2\text{O})_n$  clusters is more selective

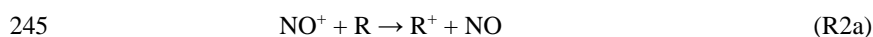


215 than the  $\text{H}_3\text{O}^+$  due to a higher PA ( $808 \text{ kJ mol}^{-1}$ , Goebbert and Wentold (2004)). This property  
216 may be valuable in our case as it allows a softer ionization of analytes. Recently Jacobs et al.  
217 (2014) have used  $\text{H}_3\text{O}^+(\text{H}_2\text{O})_n$  ions (distribution centered around  $n=4$ ) in PTR-CIMS  
218 technique with the objective of monitoring isoprene derived hydroxynitrates and their  
219 oxidation products. In order to evaluate the efficiency of the protonation mode by  
220  $\text{H}_3\text{O}^+(\text{H}_2\text{O})_n$  for the detection of other organic nitrates, a wide range of E/N ratios will be  
221 tested.

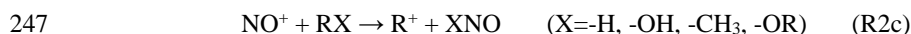
222 The  $\text{NO}^+$  chemical ionization has also been tested for the detection of organic nitrates during  
223 our experiments. It has been shown to be a complementary, sensitive and reliable method for  
224 the detection of some organic compounds such as ketones, aldehydes and alkenes by CI-MS  
225 and SIFT-MS techniques (Knighton et al., 2009; Mochalski et al., 2014; Perraud et al., 2010;  
226 Wang et al., 2004).  $\text{NO}^+$  ions are produced from the ionization of dry air within the hollow  
227 cathode discharge ion source. This process produces large amounts of  $\text{NO}^+$  with only minor  
228 amounts of  $\text{NO}_2^+$ ,  $\text{O}_2^+$ , and  $\text{H}_3\text{O}^+(\text{H}_2\text{O})_n$  impurities (Knighton et al., 2009). The intensities of  
229  $\text{O}_2^+$ , and  $\text{H}_3\text{O}^+(\text{H}_2\text{O})_n$  are quite low, less than 1% of the primary  $\text{NO}^+$  signal. In addition, it has  
230 been shown that the intensity of the  $\text{NO}_2^+$  impurity is controllable and dependant on how the  
231 hollow cathode ion source is operated (Knighton et al., 2009). The ion source extraction  
232 voltage and the hollow cathode discharge current are the two most important parameters.

233 Previous studies interrelated the PA of water to the  $\text{NO}^+$  chemical ionization binding energies  
234 (BE), creating an absolute  $\text{NO}^+$  affinity scale (Cacace et al., 1997). The study used the  $\text{H}_2\text{O}$ -  
235  $\text{NO}^+$  binding energy as a reference anchor between the two conjugated parameters and  
236 concerned various classes of ligands (alkyl halides, alkyl nitrates, alcohols, nitro-alkanes,  
237 nitriles, aldehydes, ketones, aromatic and heterocyclic compounds). With the exception of the  
238 aromatic compounds, for which the  $\text{NO}^+$   $\sigma$  type complex structures are replaced by the  $\pi$   
239 complexes, the overall data exhibit a highly correlated linear dependence ( $\text{BE}_{\text{NO}^+} = 0.367 \text{ PA}$   
240  $- 174.5 \text{ kJ mol}^{-1}$ ). When compared with protonation energies, the binding energies  
241 characterizing the  $\text{NO}^+$  chemical ionization are significantly lower (Cacace et al., 1997).

242 This characteristic offers the opportunity to generate soft ionizations with little fragmentation  
243 of the product ions, which is of high interest for the present study. Reactions which may occur  
244 are:







248 As a function of the chemical affinity, NO<sup>+</sup> chemical ionization may follow several pathways.  
 249 The charge transfer reaction (2a) seems to be the most common process for compounds  
 250 having ionization energies slightly lower or close to that of NO (IE = 9.26 eV) (e.g. isoprene  
 251 (Karl et al., 2012) butadiene, benzene (Knighton et al., 2009), monoterpenes, terpenoids  
 252 (Amadei and Ross, 2011; Rimetz-Planchon et al., 2011) and phenols (Wang et al., 2004)).  
 253 This hypothesis is confirmed by Smith et al. (2003) who reported for a series of ketones (C<sub>3</sub>-  
 254 C<sub>11</sub>) that the yields of parent radical cation increase as the IE decrease.

255 The adduct formation pathway (2b) has been previously reported for the detection of C<sub>3</sub>-C<sub>4</sub>  
 256 alkanes, alkenes and terpenes (Diskin et al., 2002; Španěl and Smith, 1998), ketones (Smith et  
 257 al., 2003; Wang et al., 2004) and flavoring esters (Iachetta et al., 2010) by selected ion flow  
 258 tube mass spectrometry. The speculated mechanism which has been proposed to explain the  
 259 formation of the adduct involves the formation of an excited intermediate complex (R·NO<sup>+</sup>)\*  
 260 which is then stabilized by collision with the carrier gas (Smith et al., 2003). Evidently the  
 261 process is enhanced at upper PTR reactor pressure involving higher collision rates.

262 A third mechanism, similar to the protonation, involves the hydride, hydroxide, methyl or  
 263 alkoxy abstraction (2c), as reported for aldehydes, ethers, alcohols (Smith and Španěl, 2005)  
 264 terpenoids (Amadei and Ross, 2011) or several unsaturated alcohols (Karl et al., 2012;  
 265 Schoon et al., 2007; Wang et al., 2004).

266 The O<sub>2</sub><sup>+</sup> ionization can generate artefacts, particularly when the PTR-MS is operated in dry air  
 267 mode, as it proceeds via a dissociative charge transfer reaction producing parent cations M<sup>+</sup>  
 268 but also fragment ions. In consequence, this process presents low interest for chemical  
 269 ionization of large molecules.

270 To summarize, several parameters will be tested in order to establish the optimal conditions  
 271 for the detection of each class of organic nitrates.

272 A thoughtful procedure was performed in order to establish the optimal measurement  
 273 conditions for each class of organic nitrates:

- 274 - First, the instrument has been used in a dual mode, employing alternatively H<sub>3</sub>O<sup>+</sup> and
- 275 NO<sup>+</sup> as a reagent ion, by shifting the GD source gas from water vapor to dry air. Dry
- 276 air was supplied to the hollow cathode ion source using the alternative GD ionization



277 line. A third operation mode which consists in suppressing the GD source gas once the  
278 plasma is established has also been tested. This last operational mode implies hence  
279 the retro-diffusion of the sampling line dry air into the GD cavity and will be further  
280 referenced as the Retro-diffusion mode (RDiff).

281 - The ions intensity and distribution are sensitive to the extraction voltage used to inject  
282 the reagent ions into the drift tube and to the hollow cathode discharge current. The  
283 PTR-MS instrument was thus operated in a wide range of E/N (electric field to number  
284 density of the gas) ratios (30 – 180 Td), hence shifting the distribution between the  
285 different ionizing analytes in the protonation mode ( $\text{H}_3\text{O}^+/\text{H}_3\text{O}^+(\text{H}_2\text{O})_n$ ) or into the dry  
286 air mode ( $\text{NO}^+/\text{NO}_2^+$ ).

287 - The sampling line and the inlet system along with the drift tube was slightly heated  
288 ( $40^\circ\text{C}$ ) and the reactor pressure ranged from 0.7 to 1.6 mbar. The sampling flow rate  
289 ( $2.9$  to  $3.5\text{ cm}^3\text{ s}^{-1}$ ) affects through the mass of the sampled analyte or through the third  
290 body collision processes the instrument response. An enhanced influence of this  
291 parameter may be noticed while operating in the RF mode.

292 - The influence of radio frequency ion funnel mode on the detection of the various  
293 organic nitrates has been tested by performing experiments with the RF mode on and  
294 off.

295 Ideally, little or no fragmentation occurs in the case of a soft ionization process. The large  
296 differences in ionization energy of the colliding species enhance the fragmentation of the  
297 organic molecule. Therefore the ionizing gas species should correspond, especially for labile  
298 molecules, to the analyte of interest in order to achieve the high yield ionizations with low  
299 excess energy.

300 In addition, the soft ionization processes demand the usage of uncommon settings of the PTR-  
301 MS device. The various effects of the altered PTR-MS tuning are termed in detail elsewhere  
302 (Hewitt et al., 2003; Knighton et al., 2009). Supplementary information relating the ion source  
303 discharge current and the extraction voltage influence are discussed in the Results section.

304 All reported signal intensities took systematically into account the background values,  
305 representing in most of the cases negligible low values of a few counts per minute.  
306 Background measurements are achieved before every single experiment by sampling the dry  
307 synthetic air of the reaction chamber.



### 308 **2.3 Normalizing analytical signal for H<sub>3</sub>O<sup>+</sup> and NO<sup>+</sup> ionization**

309 In this study, calibrated response factors of PTR-MS are determined for several types of  
310 organic nitrates in both H<sub>3</sub>O<sup>+</sup> and NO<sup>+</sup> ionization modes. For that purpose, known amounts of  
311 organic nitrates are introduced in LISA simulation chamber (see section below). To quantify  
312 the PTR-ToF-MS response factors (S; ncpm ppbv<sup>-1</sup>), the ion signal (I<sub>R+</sub>; ncpm) is divided by  
313 the known concentration of organic nitrate (ppbv<sup>-1</sup>), as measured by the FTIR in-situ  
314 technique. Corrections of the product ion signal (I<sub>R+</sub>) due to changes of the operational  
315 conditions have to be taken into account, as shown by previous studies (Knighton et al.,  
316 2009):

$$317 \quad I_{R^+} = \left( \frac{i_{R^+}}{f_{IA^+}} \right) \left( \frac{P_0}{P} \right)^2 \left( \frac{T}{T_0} \right)^2 \quad (\text{Eq. 1})$$

318 The intensity of the product ion raw signal (i<sub>R+</sub>) expressed in counts per minute is adjusted to  
319 the variabilities of the ionizing analyte (i<sub>IA+</sub>) normalized to its averaged values (⟨i<sub>IA+</sub>⟩),  
320 (f<sub>IA+</sub> = i<sub>IA+</sub>/⟨i<sub>IA+</sub>⟩; IA<sup>+</sup> = H<sub>3</sub>O<sup>+</sup> or NO<sup>+</sup>) as it has been shown that both signals (i<sub>R+</sub> and i<sub>IA+</sub>)  
321 are related. The drift tube temperature (T) and pressure (P) are also included in this expression  
322 to account for the small changes in the reaction time and gas number density that can occur  
323 during measurements. In our experiments, the temperature was very stable (± 1 K) but the  
324 PTR pressure was affected by the pressure in the simulation chamber which usually slowly  
325 decreases because of the sampling from in the constant volume of the rigid chamber.

326 Due to the high abundance of the ionizing species, the direct measurement of H<sub>3</sub>O<sup>+</sup> and NO<sup>+</sup>  
327 reagents was not possible as the ion counting signals (m/z 19 and 30) were regularly  
328 saturated. The natural isotopic abundance properties of <sup>17</sup>O (0.038% of O), <sup>18</sup>O (0.200% of O)  
329 and <sup>15</sup>N (0.368% of N) are used to overcome this drawback and evaluate the primary H<sub>3</sub>O<sup>+</sup>  
330 and NO<sup>+</sup> ion intensity using the m/z 21 (H<sub>3</sub><sup>18</sup>O) and 31 respectively (Σ <sup>15</sup>NO<sup>+</sup> and N<sup>17</sup>O<sup>+</sup>) (De  
331 Laeter et al., 2003). The I<sub>H30+</sub> = I<sub>m/z21</sub> × 500 and I<sub>NO+</sub> = I<sub>m/z31</sub> × 247 formulas were applied as a  
332 result of isotopic abundance probability calculations.

### 333 **2.4 LISA Atmospheric Simulation Chamber.**

334 Gaseous mixtures of organic nitrates at the ppb-ppm level were generated in the simulation  
335 chamber at LISA. This chamber comprises a Pyrex reactor of 977 L equipped with a multiple  
336 reflection optical system interfaced to a FT-IR spectrometer (Vertex 80 from Bruker). Details  
337 of this smog chamber are given elsewhere (Doussin et al, 1997).



338 All experiments were conducted in the dark at  $298 \pm 2$  K and atmospheric pressure. Mixtures  
339 of organic nitrates were generated in synthetic air ( $N_2$  80% +  $O_2$  20%) by introducing a  
340 known amount of the organic nitrate into the chamber and cross-monitored by long path *in*  
341 *situ* FTIR and PTR-MS techniques. Concentrations of organic nitrates were checked from  
342 their infrared spectral absorption bands. Integrated Band Intensities (IBIs; expressed in  $cm^2$   
343  $molecule^{-1}$  and calculated in decimal logarithm) and the spectral integration areas used to  
344 quantify PAN like compounds and other nitrates are:  $9.50 \times 10^{-18}$  for PANs ( $765\text{--}812\text{ cm}^{-1}$ ),  
345  $8.30 \times 10^{-18}$  for alkyl nitrates ( $820\text{--}900\text{ cm}^{-1}$ ),  $1.17 \times 10^{-17}$  for hydroxynitrates ( $816\text{--}882\text{ cm}^{-1}$ ),  
346  $1.08 \times 10^{-17}$  for ketonitrates ( $820\text{--}870\text{ cm}^{-1}$ ). The IBIs values are given by the Beaver et al.  
347 (2012) and Bates et al. (2014) studies for the PANs and the hydroxynitrates respectively,  
348 whereas for the alkyl nitrates and ketonitrates the IBIs were calculated from repetitive  
349 injections of known amount of analyte, in the current study. Worth notice the weak disparity  
350 of cross sections concerning the characteristic  $-ONO_2$  absorption band.

351 Before and after every single experiment, a cleaning procedure was applied in order to avoid  
352 memory effects from an experiment to the next one. It consists in vacuum clean-up down to  
353  $10^{-2}$  mbar for at least 10h and UV irradiation (340 and 360 nm fluorescent tubes) in order to  
354 heat the reactor and improve desorption of semi and low volatile compounds from the walls.

355

## 356 2.5 Chemicals and gases

357 The simulation chamber was filled with dry synthetic air generated with  $N_2$  (from liquid  
358 nitrogen evaporation, >99.995% pure, <5ppm  $H_2O$ , Linde Gas) and  $O_2$  (quality N45,  
359 >99.995% pure, <5 ppm  $H_2O$ , Air Liquide). Supplementary cylinder air was used for the dry  
360 air glow discharge generation in PTRMS (ALPHAGAZ™ 2;  $H_2O$  < 0,5 ppm;  $C_nH_m$  < 50 ppb;  
361  $CO_2$  < 0,1 ppm;  $CO$  < 0,1 ppm;  $NO_x$  < 10 ppb)

362 The alkyl nitrates considered in the present study (n-propyl nitrate - 97% Janssen Chimica;  
363 AlkC3 and isobutyl nitrate - 96 % Sigma Aldrich; AlkiC4) were used as commercially  
364 available, without further purification.

365 Ketonitrates were synthesized using Kames' method, (Kames et al., 1993): a liquid/gas phase  
366 reaction in which the corresponding hydroxyketone is reacted with  $NO_3$  radicals released  
367 from the dissociation of  $N_2O_5$ , at ice bath temperature, under dry condition. The carbonyl



368 nitrates and nitric acid were separated by multiple headspaces vacuum procedure. The  
369 carbonyl nitrates' structure and purity were verified by FT-IR. The presence of HNO<sub>3</sub> is  
370 regularly noticed as injected as by product of the carbonyl nitrates synthesis. 1-hydroxy-2-  
371 propanone (95% Alfa Aesar) and 3-hydroxy-3-methyl-2-butanone (97% Sigma Aldrich) were  
372 used for the synthesis of 1-nitroso-2-propanone and 3-nitroso-2-propanone respectively.

373 The hydroxynitrate was synthesized starting from the commercially available 3-bromo-1-  
374 propanol (97% Sigma Aldrich). Its conversion to the analog iodide was performed by a  
375 Finkelstein reaction with sodium iodide (Baughman et al., 2004) and the subsequent mild  
376 conversion with AgNO<sub>3</sub> (Castedo et al., 1992) leads to the formation of 1-hydroxy-3-nitroso-  
377 propane (1OH3C3).

378 The PAN type compounds were generated in the simulation chamber from the gas-phase  
379 oxidation of corresponding aldehydes by NO<sub>3</sub> radicals (Hanst, 1971). In our experiments,  
380 peroxyacetyl nitrate (PAN) was formed from the oxidation of acetaldehyde (>99.5% Sigma  
381 Aldrich). This reaction has been shown to produce mainly PAN with a yield close to 70%  
382 (Doussin et al., 2003).

### 383 **3 Results and discussion**

#### 384 **3.1 Influence of the operating conditions on the ionizing analytes signals**

385 As already termed, intensities and mixing ratios of the ionizing species are dependent on the  
386 E/N ratio. For a standard drift tube, E/N is a well-defined quantity but when the instrument is  
387 run in RF mode, the influence of the additional ac electric field on the E/N ratio has to be  
388 taken into account and this is not obvious. Barber et al, 2012 have attempted to empirically  
389 estimate an effective E/N by running the instrument with the RF mode on and off and by  
390 seeking operating conditions for the RF mode on that match the performance obtained when  
391 the RF mode is off. The criterion used to estimate the performance is the ratio  
392  $[H_3O^+]/[H_3O^+(H_2O)]$ . During our experiments, the additional ac electric field was fixed. Thus,  
393 variations of E/N ratio result only from variations of the dc component of the drift tube.

394

395 Typically recorded distributions over a relevant range of E/N are illustrated in *Figure 1* for  
396 both ionization modes, with and without the above described RF mode. When the RF mode is  
397 not employed, the water cluster ion distribution obtained in this study (*Figure 1*) is in



398 reasonable agreement with those calculated and measured by de Gouw and Warneke (2007)  
399 asserting that i) the  $\text{H}_3\text{O}^+(\text{H}_2\text{O})_2$  cluster is abundant for E/N ratios  $< 60\text{Td}$ , ii) the  $\text{H}_3\text{O}^+(\text{H}_2\text{O})$   
400 signal is maximum around  $80\text{Td}$  and iii) the  $\text{H}_3\text{O}^+$  signal is predominant for values larger than  
401  $100\text{Td}$ . In the RF mode, it has been observed that the signal of  $\text{H}_3\text{O}^+$  ion is much higher than  
402 those of clusters for the entire range of E/N ratios. The  $\text{H}_3\text{O}^+(\text{H}_2\text{O})$  is one order of magnitude  
403 lower than the  $\text{H}_3\text{O}^+$  and one order of magnitude more abundant than the  $\text{H}_3\text{O}^+(\text{H}_2\text{O})_2$ . As the  
404 distributions of ions obtained with and without RF mode are quite different, it was not  
405 possible to estimate an effective E/N as proposed by Barber et al., 2012. So E/N ratios have  
406 been calculated without taking into account the RF contribution. In the case the RF mode is  
407 on, E/N ratios are indicated with \* (E/N\*).

408 The  $\text{NO}^+$  ionization mode has been found more promising in the RF mode, since the  
409 abundance of the ionizing species is largely superior. Furthermore, the  $\text{NO}^+/\text{NO}_2^+$  ratio  
410 exhibits the highest values around  $40\text{Td}$  in the RF mode, increasing the probability to form  
411 the analyte- $\text{NO}^+$  adduct. Therefore, all further results presented in the current work in the  $\text{NO}^+$   
412 mode have been recorded with the RF mode and reported E/N\* were calculated without  
413 taking into account the ac radiofrequency contribution.

## 414 3.2 Alkyl-nitrates

### 415 3.2.1 $\text{H}_3\text{O}^+$ ionization mode

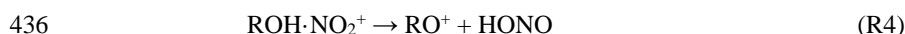
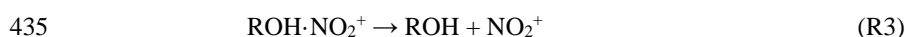
416 A series of tests has been conducted in order to seek the optimum operating conditions for the  
417 measurement of alkyl nitrates with  $\text{H}_3\text{O}^+$  ionization mode. In particular, the E/N ratio was  
418 spanned in the  $50\text{-}140\text{ Td}$  range. The intensity of the main signals obtained for n-propyl  
419 nitrate (AlkC3) with the RF mode off has been plotted as a function of E/N in *Figure 2*. The  
420 recorded mass spectra of AlkC3 are characterized by a high degree of fragmentation, even for  
421 the lowest E/N ( $50\text{ Td}$ ). The AlkC3 mass spectra recorded at the lowest extent of  
422 fragmentation of the protonated molecular ion is illustrated by *Figure S1 in S.I.*. The same  
423 result has been observed for AlkC4. Consequently, the sensitivity of the molecular ions  
424 formed is low (see Table 2). The protonated alkyl nitrates are expected to adopt the ion-dipole  
425 complex conformation ( $\text{ROH}\cdot\text{NO}_2^+$ ; R1a) and not a covalently bound  $\text{RONO}_2\text{H}^+$  one (Cacace  
426 and de Petris, 2000).





428 The bound energy of these complexes was calculated by *ab initio* methods to be around 82 kJ  
429 mol<sup>-1</sup> in the case of methyl nitrate (Lee and Rice, 1992).

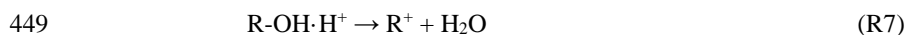
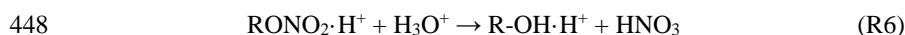
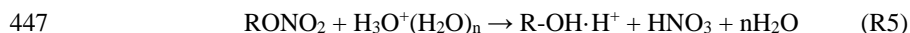
430 The only other study (Aoki et al., 2007) describing a tentative of alkyl nitrate detection with  
431 PTR-MS used E/N ratio spanning in between 96 and 147 Td. The low BE characterizing the  
432 formed complex enables its decomposition in ROH and NO<sub>2</sub><sup>+</sup> by collision induced  
433 dissociations. The recorded signals of NO<sub>2</sub><sup>+</sup> (m/z 46) and RO<sup>+</sup> (m/z 59 for AlkC3 and 73 for  
434 AlkiC4) are probably formed by the mechanisms:



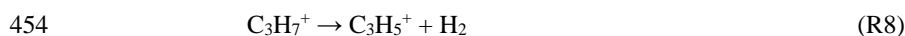
437 This statement is supported by the decrease of the protonated signal in conjunction with the  
438 increase of the NO<sub>2</sub><sup>+</sup> with increasing E/N.

439 The presence of the m/z 43 (AlkC3) and respectively 57 (AlkiC4) signal was clearly  
440 identified as the alkyl fragment (R<sup>+</sup>) of nitrate by the means of high resolution mass  
441 spectrometer allowing to differentiate between oxygen containing analytes and alkyl  
442 fragments.

443 Due to the abundance of water clusters, higher in our study than typically, the R5 mechanism  
444 is considered more likely, as proposed by Aoki et al. (2007). The formation of R-OH·H<sup>+</sup> ion  
445 can also be explained by reaction R6 as proposed by Spanel and Smith (1997) This ion is then  
446 expected to form the alkyl fragment (R<sup>+</sup>) by reaction R7:



450 A third option is to consider the direct formation of the alkyl fragment from the collision  
451 induced dissociation of the protonated alkyl nitrates formed in reaction 1a into R<sup>+</sup> and HNO<sub>3</sub>.  
452 Further collisions of the alkyl fragment (R<sup>+</sup> = C<sub>3</sub>H<sub>7</sub><sup>+</sup>) might generate the loss of two  
453 hydrogens and explain the weak signals at m/z 41 in the case of AlkC3.



455 It should be noticed that the analog process for the m/z 55 in the case of AlkiC4 cannot be  
456 observed since it falls nearby a relatively abundant water cluster signal.



457 Results obtained with the RF mode are shown in Figure 3 for the AlkC3. The ionization  
458 pattern of the analyte is slightly different from the one obtained without RF mode and  
459 enables, adjacent to the formation of the protonated alkyl nitrate, the identification of other  
460 specific signals like the adduct  $\text{AlkC3}\cdot\text{H}_3\text{O}^+$  formation. Characterized by a high degree of  
461 fragmentation, the spectra contain the protonated ion-dipole complex  $\text{ROH}\cdot\text{NO}_2^+$  at  $m/z = 106$   
462 (R1a) with the highest sensibility above 60Td. The E/N ratio is calculated without taking into  
463 account the RF contribution. The  $m/z$  124 signal can be assigned to the  $\text{AlkC3}\cdot\text{H}_3\text{O}^+$  adduct  
464 formation. An analog process is described in the literature for long alkanes ( $> \text{C}_6$ ) providing  
465  $\text{M}\cdot\text{H}_3\text{O}^+$  signals (Španěl and Smith, 1998), in contrast with the alkenes which are readily  
466 protonated due their higher PA.

467 The alkyl ( $\text{R}^+$ ) intermediary parent ion, described in R5 and R6 ( $\text{R}\cdot\text{OH}\cdot\text{H}^+$ ) is equally  
468 recorded, corresponding in the case of AlkC3 to the  $m/z$  61 signal. The increase of the E/N  
469 ratio over 60Td contributes to a higher degree of decay of this intermediate ion in the  
470 particular conditions of the RF mode. The  $\text{RO}^+$  ion at  $m/z$  59 is equally present in the case of  
471 AlkC3 confirming the existence of the R4 mechanism conducting to HONO formation.

472 To summarize, the use of  $\text{H}_3\text{O}^+$  ionization is not really suitable for the detection of alkyl  
473 nitrates as it leads to high fragmentation, even at low E/N ratios, hence generating intense  
474 signals of common organic analytes, unsuitable for a reliable identification of these  
475 compounds. In addition, if considering the more characteristic signals of the protonated ion-  
476 dipole complex  $\text{ROH}\cdot\text{NO}_2^+$ , the  $\text{H}_3\text{O}^+$  ionization mode exhibits poor detection limit: 5 ppb  
477  $\text{min}^{-1}$  for both AlkC3 ( $m/z$  106) and AlkiC4 ( $m/z$  120). This detection limit was estimated for  
478 a mean signal/noise ratio of 3 at the chosen  $m/z$ .

479 In Table 2, are gathered the characteristic signals of each organic nitrate studied here as well  
480 as their detection limits.

481

### 482 3.2.2 $\text{NO}^+$ ionization mode

483 The performances of the  $\text{NO}^+$  ionization were also evaluated. The most promising results,  
484 enabling the identification of characteristic signals of the studied alkyl nitrates, were obtained  
485 in the RF mode. The scan of a large range of E/N\* ratios confirmed that the highest sensibility  
486 towards  $\text{NO}^+$  induced ionization and identification is obtained around 40Td as illustrated in





487 Figure 3 for the AlkC3 case. As mentioned previously, the calculated E/N ratio does not take  
488 into account the RF contribution to the ion funnel field.

489 The recorded mass spectra of the analyte of interest in terms of relative peak intensities as a  
490 function of the  $m/z$  are represented by the thick black lines in Figure 4. It will be kept in mind  
491 that the  $\text{NO}^+$  and  $\text{NO}_2^+$  signals illustrated above are the sum of the corresponding nitrate  
492 fragments as well as the ions formed into the dry air plasma GD. The presence of  $\text{O}_2^+$  ( $m/z =$   
493 32) and its interfering isotopic abundance signals at  $m/z = 33$  and 34 has been observed and  
494 could result in interfering signals.

495 For both alkyl nitrates, the adduct formation (2b) appears to be the main ionization  
496 mechanism under these given conditions, leading to intense peaks at  $m/z = 135$  ( $105+30$ ) and  
497  $m/z = 149$  ( $119+30$ ) for AlkC3 and AlkC4 respectively (see Figure 4 and Figure S2). The  
498 hydride abstraction ( $\text{R}(-\text{H})^+$ ) was also detected as a minor pathway (2c) at  $m/z = 104$  and  $m/z$   
499  $= 118$  for AlkC3 and AlkC4 respectively. Despite a weak intensity, this signal can be used as  
500 an interrelated identification signal for alkyl nitrates. The fraction of the abstraction channel is  
501 at no time higher than 10% of the intensity of the adduct formation channel.

502 An intense peak corresponding to the alkyl fragment ( $\text{R}^+$ ) was observed in spectra at  $m/z$  43  
503 (AlkC3) and 57 (AlkC4). The alkyl fragment signal is followed by a downward series of  
504 signals at  $m/z$  41 and 39 in the case of AlkC3 and at  $m/z$  55 and 53 for the AlkC4.  
505 Considering the collisions of the alkyl fragment mechanism generating the loss of two  
506 hydrogens (R8), as proposed by Aoki et al. (2007) for the protonation mode, could explain the  
507 recorded signals.

508 In conclusion, the  $\text{NO}^+$  ionization mode appears to be more suitable for the detection of alkyl  
509 nitrates than the  $\text{H}_3\text{O}^+$  ionization mode as it produces two characteristic signals,  
510 corresponding to the adduct formation ( $\text{M.NO}^+$ ) and the hydride abstraction ( $\text{M}(-\text{H})^+$ ). The  
511 detection limit for the  $\text{M.NO}^+$  signal was estimated to be  $205 \text{ ppt min}^{-1}$  for AlkC3 ( $m/z$  135)  
512 and  $126 \text{ ppt min}^{-1}$  in the case of AlkC4 ( $m/z$  149) (see Table 2). Although superior to the  
513 protonation mode, the  $\text{NO}^+$  ionization exhibits a poor sensitivity. For measurements in real  
514 atmosphere where alkyl nitrates mixing ratios are usually in the ppt level, accumulations for  
515 several hours will be necessary.

516



### 517 3.3 Hydroxy-nitrates

#### 518 3.3.1 The $\text{H}_3\text{O}^+$ ionization

519 As for alkyl nitrates, the measurement of hydroxy-nitrates by PTR-MS has been tested with  
520  $\text{H}_3\text{O}^+$  ionization mode, with and without RF mode. For this purpose, 1-hydroxy-3-nitroxy-  
521 propane ( $\text{1OH3C3}$ ) was synthesized and used as template. In the classical mode (RF off), the  
522 main signals which have been attributed to  $\text{1OH3C3}$  are:  $m/z$  43 ( $\text{C}_2\text{H}_3\text{O}^+$ ),  $m/z$  104  
523 ( $\text{M}_{\text{1OH3C3}}(-\text{OH})^+$ ),  $m/z$  122 ( $\text{M}_{\text{1OH3C3}}\cdot\text{H}^+$ ),  $m/z$  139 ( $\text{M}_{\text{1OH3C3}}\cdot\text{H}_2\text{O}^+$ ). Intensities of these  
524 signals have been plotted as a function of E/N in *Figure 5*. As expected, the intensity of the  
525 signal  $m/z$  43 increases with high E/N ratio while protonation and water adduct formation are  
526 favored by low E/N. A possible explanation for the formation of the ion  $\text{M}_{\text{1OH3C3}}(-\text{OH})^+$  is a  
527 loss of  $\text{H}_2\text{O}$  after protonation of the hydroxyl-nitrate, as suggested by several studies for  
528 alcohols (Schoon et al., 2007; Smith et al., 2012; Tuazon et al., 1999).

529 When the RF mode is on, the same signals (43, 104, 122, 139) were observed but with  
530 different relative abundance. The influence of E/N on the intensity of these signals has been  
531 plotted in *Figure 6*. Above 40 Td, the signal characterizing the water adduct formation ( $m/z$  =  
532 139) is more abundant in the RF mode with a maximum around 45Td.

533 The water clusters are probably abundant in the PTR reactor due to the low E/N ratios and  
534 dissociate only into the RF region after the ionization occurs.

535 The mass spectrum illustrated by *Figure S3* was recorded in absence of the RF funnel and is  
536 dominated by fragments like  $m/z$  59, 60, 73, while the specific signal of the protonated  
537 molecule  $m/z$  122 is present close to the noise limit.

538 The above described water adduct formation ( $m/z$  = 139) is competed by a  $\text{H}_3\text{O}^+$  adduct ( $m/z$   
539 = 140), equally present into the spectra. The ionization is probably induced by the expected  
540 high levels of water cluster, following an analogous process with the one described in R5.  
541 This involves the release of  $\text{HNO}_3$  and arise the signal at  $m/z$  77 ( $\text{C}_3\text{H}_6\text{OH}-\text{OH}\cdot\text{H}^+$  and  
542 subsequently at  $m/z$  59 with the loose of supplementary water (R7). Further collisions of the  
543 above mentioned ions may well explain the signals at  $m/z$  75 and 57, generated by the loss of  
544 two hydrogens (R8).

545 In RF mode, the mass spectrum obtained for  $\text{1OH3C3}$  at  $\text{E/N}^* = 45$  Td (corresponding to the  
546 operational condition for which the signal at  $m/z$  139 is the most intense) was illustrated in



547 *Figure 7.* It is worth to notice that all the other competitive ionization processes are strongly  
548 diminished in comparison to the spectrum obtained in classical mode. Only the specific signal  
549 at  $m/z = 104$  exhibit a stronger signature compared to the case above. The fragmentation  
550 pattern is strongly diminished in this case.

551 To conclude, it has been observed that protonation of the hydroxynitrate is a minor process in  
552 comparison to fragmentation and to adduct formation. The use of the RF mode significantly  
553 reduces the fragmentation for the benefit of the  $M.H_2O^+$  adduct formation. The lowest DL (80  
554  $ppb\ min^{-1}$ ) was obtained at 45Td\* in the RF mode for the signal corresponding to the water  
555 adduct formation at  $m/z$  139. The same signal in absence of the RF effect is at least twice  
556 weaker in terms of sensibility. Sensitivities of other specific signals are equally proposed for  
557 comparison in Table 2.

### 558 3.3.2 The $NO^+$ ionization

559 The detection of hydroxy-nitrates in  $NO^+$  ionization mode has been evaluated for the first  
560 time, by varying the E/N ratio (39 – 44 Td) and by studying the influence of the RF mode. As  
561 stated before the highest sensibility towards the  $NO^+$  adduct formation are obtained in the RF  
562 mode, most likely due to the higher abundance of the ionizing species, as already seen in  
563 Figure 1.

564 Results obtained with RF mode have shown in *Figure 8.* Main signals which have been  
565 observed are: 151 and 167 which have been attributed to  $M.NO^+$  and  $M.NO_2^+$  adducts  
566 formation and 43 ( $C_2H_3O^+$ ) which is characteristic of fragmentation. Although weak, the  
567 hydride abstraction (R2c) leading to a signal at  $m/z$  120 has also been observed in the  
568 recorded spectra. This process has already been observed in previous studies for various  
569 saturated and unsaturated alcohols ( $C_{1-10}$ ) and phenol (Karl et al., 2012; Schoon et al., 2007;  
570 Spanel and Smith, 1997) using SIFT and PTR-MS techniques. The hydride ion transfer of  
571 these compounds generates the corresponding carboxy ion (and HNO), while the hydroxide  
572 ion transfer gives the corresponding hydrocarbon ion (and  $HNO_2$ ). Assuming the  
573 corresponding ionization of hydroxynitrate in the case of the 1OH3C3, would involve the  
574 formation of the  $(O_2NO-C_3H_6)-O^+$  at  $m/z$  120 and  $(O_2NO-C_3H_6)^+$  at  $m/z$  104 but their spectral  
575 signature is marginal into the spectra.



576 As expected, the intensity of the signal 43 increases with increasing E/N ratio. The opposite  
577 tendency was observed for adducts. The mass spectrum obtained at  $E/N^* = 41$  which  
578 corresponds to the highest sensitivity for the  $m/z$  151 signal is shown in *Figure 9*.

579 Beside the above mentioned characteristic signals, other specific mechanisms could be  
580 associated to the spectral signature of 1OH3C3. The mechanism is reviewed and suggested by  
581 (Harrison, 1999) for the particular case of  $\text{NO}^+$  ionization of primary alcohols. In this study,  
582 an additional product ( $\text{R}(-2\text{H}) + \text{NO}^+$ ) has been observed which would correspond in our case  
583 to an  $m/z = 149$ , hypothetically formed by the oxidation of the alcohol to the corresponding  
584 aldehyde and its subsequent ionization. Although relatively weak the signal is systematically  
585 recorded in the mass spectra of the hydroxy-nitrate. The 45 and 67 ions are equally present in  
586 mass spectra and can be attributed to fragmentation.

587 The detection limit obtained in  $\text{NO}^+$  ionization mode at E/N ratio of 41 Td\* for the  $\text{M.NO}^+$   
588 signal at  $m/z$  151 was quite low (37 ppt.min<sup>-1</sup>) showing that this ionization mode is more  
589 suitable than  $\text{H}_3\text{O}^+$  mode for the measurement of hydroxy-nitrates. As shown in Table 2, the  
590 hydrogen abstraction signal ( $m/z$  120) is at least one order of magnitude less sensitive.

591

## 592 **3.4 Keto-nitrates**

### 593 **3.4.1 The $\text{H}_3\text{O}^+$ ionization**

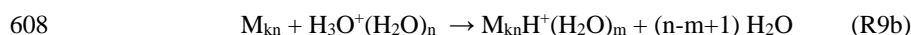
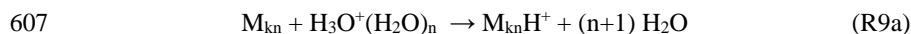
594 Two distinct keto-nitrates were synthesized and characterized in the current study, 3-nitroxy-  
595 2-propanone (KnC3) and the 3-nitroxy-3-methyl-2-butanone (KnC5).

596 In order to identify the optimal conditions for the detection of ketonitrates in  $\text{H}_3\text{O}^+$  ionization  
597 mode, tests were performed by varying E/N ratios into a large domain, from 45 to 170 Td  
598 (*Figure 10*).

599 Several signals which can be attributed to keto-nitrates have been detected, as illustrated in  
600 *Figure 10* for KnC3: At low E/N ratios, which correspond to the  $\text{H}_3\text{O}^+(\text{H}_2\text{O})_2$  controlled  
601 regime, the formation of two keto-nitrate water cluster adducts,  $\text{M}_{\text{kn}}\cdot\text{H}_3\text{O}^+$  ( $m/z=138$ ) and  
602  $\text{M}_{\text{kn}}\cdot\text{H}_3\text{O}^+(\text{H}_2\text{O})$  ( $m/z=156$ ) has been observed. Worth notice the reduction of these specific  
603 signals with the decay of the preeminent ionizing analyte  $\text{H}_3\text{O}^+(\text{H}_2\text{O})_2$  ( $m/z= 55$ ) signal. The  
604 literature available data expect that for polar compoundsthe ionization process may follow



605 two similar pathways, by proton-transfer (R9a) and by ligand-switching reaction (R9b) (de  
 606 Gouw et al., 2003).



609 The bound energy of the cluster ions formed in the reaction above (R9b) is weaker than the  
 610 water cluster bond. In the given conditions, there is a high probability that the drift tube  
 611 dissociative effect can split the formed cluster ions and lead to the formation of  $MH^+$  and  
 612  $MH^+(H_2O)$ . Since the cluster ion distribution may be governed by the water vapor drift tube  
 613 loads, the detection efficiency can be humidity reliant in this particular case (de Gouw et al.,  
 614 2003).

615 Redistribution processes among the various precursor ions formed into the glow discharge can  
 616 equally occur, leading to the formation of auxiliary hydrated ions such as  $NO^+(H_2O)_n$ , able to  
 617 produce ligand-switching reactions alike the ones presented above (R9b).

618 For intermediate E/N ratios, where  $H_3O^+(H_2O)$  water cluster is the key analyte, we notice that  
 619 the signal corresponding to  $M_{kn} \cdot H^+$  ( $m/z=120$ ) is maximum. In addition, two other signals  
 620 corresponding to  $M_{kn} \cdot NO^+$  ( $m/z=149$ ) and  $M_{kn} \cdot NO_2^+$  ( $m/z=165$ ) adducts formation have also  
 621 been observed and rise up to a maximum for these intermediate E/N ratios. These adducts can  
 622 be explained by the formation of  $NO^+$  and  $NO_2^+$  analytes in the GD, which increases with the  
 623 increasing E/N ratios.

624 For high E/N ratios, the  $m/z$  43 ( $C_2H_3O^+$ ) signal which is a common fragment of organic  
 625 compounds, strongly increases. This reveals that mainly fragmentation occurs, making this  
 626 region not suitable for the detection of ketonitrates.

627 From these results, the intermediate E/N ratios (70 - 80 Td) appear to be the most suitable for  
 628 the detection of keto-nitrates in  $H_3O^+$  ionization mode. Mass spectra obtained at  $E/N=75$ Td  
 629 which corresponds to the highest sensibility of the  $M_{kn} \cdot H^+$  signal are shown in *Figure 11* for  
 630 KnC3 and in S.I. Figure S4 for KnC5 respectively.

631 For KnC3, the most intense signal corresponds to  $M_{kn} \cdot H^+$  ( $m/z=120$ ). As discussed above,  
 632 additional processes occur which are responsible for other signals:  $M_{kn} \cdot NO^+$  adduct formation  
 633 at  $m/z$  149 and fragmentation at  $m/z$  43 ( $C_2H_3O^+$ ). These characteristic signals are tailed by  
 634 their corresponding isotopic abundance signals mainly due to  $^{13}C$  isotope at  $m/z=121$  and 150.



635 The already discussed reactions R5 and R6 could explain the intense signal of  $m/z$  75 since  
636 the resulting  $(C_3H_5O)-OH \cdot H^+$  ion seems the accurate match of this signal.

637 Worth notice that due to the low  $E/N$  ratios, imposed by the breakability of organic nitrates, in  
638 the above illustrated mass spectra examples, the intensities of the signals  $m/z$  19 ( $H_3O^+$ ) and  
639 37 ( $H_3O^+(H_2O)$ ) are of the same order of magnitude while the  $m/z$  55 ( $H_3O^+(H_2O)_2$ ) is one or  
640 two orders of magnitude lower.

641 In the case of  $KnC_5$ , the  $M_{kn} \cdot H^+$  ( $m/z=148$ ) signal is not the most intense one, suggesting that  
642 fragmentation is more favored than for  $KnC_3$  under similar conditions. The characteristic  
643 fragmentation pattern of this analyte exhibits a characteristic  $m/z$  85 signal corresponding to  
644 the  $C_5H_9O^+$  group after the cleavage of the  $NO_3$  fragment. An analogous process is described  
645 by Aoki et al. (2007) asserting the alkyl group as the main signal in the mass spectra of alkyl  
646 nitrates. The abundant  $m/z$  59 fragment ( $C_3H_7O^+$  or  $C_2H_3O_2^+$ ) is most probably a result of  
647 subsequent fragmentation/recombination processes.

648 The intense  $m/z=103$  signal could be ascribed to the already mentioned R5 and/or R6, both  
649 conducting to the formation of a  $(C_5H_9O)-OH \cdot H^+$  ion with release of  $HNO_3$  and water. Worth  
650 notice that the elimination of supplementary  $H_2O$  from the resulting complex could also  
651 contribute to the  $m/z$  85 signal ( $C_5H_9O^+$ ).

652 In the RF mode, the water clusters distribution is dominated by the  $H_3O^+$  ion, for the entire  
653 range of  $E/N^*$  ratios. Its signal is the most abundant, while all the other  $H_3O^+(H_2O)_n$  species  
654 are at least one order of magnitude lower. The redistribution of water cluster in the RF mode  
655 modifies obviously the keto-nitrates' fragmentation pattern and the burden of each ionization  
656 channel in a similar way as in the case of hydroxy-nitrates. No straightforward correlation can  
657 be made in between the two modes, showing the complexity of the ion funnel influence.

658 The most noteworthy difference in the RF mode resides in the presence of an intense signal  
659 corresponding to a  $H_2O$  adduct formation ( $m/z$  137 and 165 respectively), similar to the  
660 hydroxy-nitrate, with a maximum intensity around 48 Td (Table 2) as calculated without  
661 taking into account the RF contribution.

662 With the same PTR entry voltage, the RF mode activation induces the enhancement of the  
663 fragmentation due to higher input energies and the maximum of the protonated ketonitrate  
664 signal glides towards 48 Td. Making the assumption that the highest sensibility is related in  
665 the two modes to an analogous  $E/N$  state, a coarse assessment of the RF mode contribution is



666 estimated (25 - 35 Td) as the difference between the two modes maximum sensibility for the  
667 protonated molecular ion signal.

668 To conclude, it has been observed that protonation of ketonitrates is the main ionization  
669 process in the absence of a RF field. The use of the RF mode modifies the fragmentation  
670 pattern and enhances the mechanism leading to the  $M.H_2O^+$  adducts formation. The recorded  
671 sensitivities listed in Table 2 for the  $H_3O^+$  ionization mode, to a DL of 70 - 80 ppt  $min^{-1}$  for  
672 the protonated signal of KnC3 ( $m/z$  120). A similar DL is reached by the water adduct signal  
673 at  $m/z$  137 under the influence of the RF ion funnel. The highest sensibility for the KnC5  
674 identification is attained by the water adduct signal at  $m/z$  165 recorded at 48Td in the RF  
675 mode with a DL of 20 ppt  $min^{-1}$ . Sensitivities of other specific signals are equally proposed  
676 for comparison in Table 2.

### 677 3.4.2 The $NO^+$ ionization

678 For the first time, the detection of keto-nitrates using  $NO^+$  ionization was tested. In a similar  
679 way as for the protonation process, mass spectra of KnC3 and KnC5 were recorded as a  
680 function of E/N ratios. The previously proven affinity of  $NO^+$  coupling -C(O) functional  
681 group in ketones to form adducts (Smith et al., 2003) was for the first time tested in a PTR  
682 reactor. The adduct formation was successfully achieved in the presence of  $NO^+$  for both  
683 studied ketonitrates, for which very similar IE are expected.

684 In the given ionization mode and considering the higher IE of ketonitrates, the adduct  
685 formation is expected to prevail over the charge transfer, the literature stating that the yield of  
686 parent radical cation formation seems to be anti-correlated with the IE of the ketones, the  
687 lowest IE analytes, presenting the highest probability for the charge transfer reaction (Smith et  
688 al., 2003).

689 Following the same approach as in the previous case, the E/N\* region was set in order to  
690 provide the highest  $NO^+/NO_2^+$  ratio. The *Figure 12* is presenting the influence of the E/N ratio  
691 variation in the RF mode over the analyte signal of interest. We notice that the  $NO^+$  profile  
692 sharply increasing together with the  $NO^+/NO_2^+$  ratio is joint by the adduct signal.

693 We plot as an example, the KnC5 adduct signal at  $m/z=177$  ( $147+30$ ) as a function of two  
694 fragments ( $m/z= 43$  and  $85$ ) having potentially, as explained above, different formation  
695 pathways. A decrease of the fragmentation yield in favor of the adduct formation in the PTR



696 reactor is observed over the 35 Td shoulder. The high sensitivity of the instrumental setup for  
697 the identification of ketonitrates is quantified in Table 2.

698 Due to the rising incidence of the  $\text{NO}^+$  and  $\text{NO}_2^+$  ions, simultaneously formed in the GD, the  
699 signals corresponding to the  $\text{M}_{\text{kn}}\cdot\text{NO}^+$  and  $\text{M}_{\text{kn}}\cdot\text{NO}_2^+$  adducts formation is equally  
700 strengthened ( $m/z=149$  and  $165$  for the  $\text{KnC3}$  - *Figure 13* and  $m/z=177$  and  $193$  for the  $\text{KnC5}$   
701 – see S.I. Figure S5 respectively). All these characteristic signals are tailed by their  
702 corresponding isotopic abundance signals due mainly to  $^{13}\text{C}$  isotope at  $m/z=121$ ,  $150$ ,  $166$ ,  
703  $178$  and  $194$  respectively.

704 The  $\text{KnC3}$  spectrum was recorded at  $E/N^* = 40\text{Td}$  as shown in *Figure 13*. We notice a low  
705 fragmentation pattern of the analyte with a major adduct signal contribution at  $m/z= 149$ . The  
706 existence of a secondary (water controlled) competitive process might be revealed by the  
707 existence of the minor protonated signal at  $m/z$  120 backed by the characteristic fragment at  
708  $m/z =75$  as described by R5-7.

709 In an analog way, in S.I. *Figure S5*, the mass spectrum of  $\text{KnC5}$  is plotted for the instrumental  
710 setup corresponding at the lowest fragmentation ( $E/N = 36$  Td). We notice the distinct signal  
711 of the formed adduct ( $m/z =177$ ) as well as, to a lower extent, the characteristic signals  
712 described above ( $m/z= 59$ ,  $85$ ,  $103$ ) which are most likely formed following the mechanisms  
713 described in the previous paragraph, since the water is ubiquitously present in the system.

714 The best results related to the  $\text{NO}^+$  ionization are related typically to the highest  $\text{NO}^+/\text{NO}_2^+$   
715 ratios in the RF mode as seen in Table 2. The  $\text{NO}^+$  high affinity towards adduct formation is  
716 confirmed by the low DL achieved for these highly characteristic signals,  $30$  and  $40$   $\text{ppt min}^{-1}$   
717 for the adducts formed at  $m/z$   $149$  and  $177$  respectively at an  $E/N^*$  ratio  $< 45$  Td.

718

### 719 3.5 PANs

720 The detection of PANs with PTR-MS has been tested by generating the peroxyacetyl nitrate  
721 (PAN) from the well-known  $\text{NO}_3$ -oxidation of acetaldehyde in the simulation chamber. The  
722 disadvantage of this procedure despite the 70% PAN formation yield (Doussin et al., 2003) is  
723 that it generates several bi-products (nitric acid, formaldehyde...) leading to more complex  
724 mass spectra. The PANs family analytes were all obtained by in-situ generation using the  
725 corresponding aldehydes. In order to overcome any judgment error, the present study will



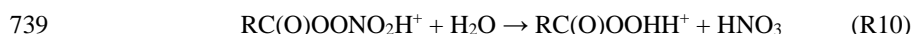


726 only illustrate the PAN mass spectra while for the other analogous formed PAN like products  
 727 (P2MCrN and P3MCrN) we will only discuss about the mass spectra signals which are  
 728 assigned to them.

### 729 3.5.1 The H<sub>3</sub>O<sup>+</sup> ionization

730 The optimal conditions for the detection of PANs in H<sub>3</sub>O<sup>+</sup> ionization mode were explored by  
 731 varying the E/N ratios from 55 to 120 Td. The most promising results were obtained in the  
 732 case of PAN around 85Td where the protonated signal of PAN was recorded as we can depict  
 733 from Figure S6 in S.I.

734 In an analogous way with the reaction R1a, the protonated peroxy-nitrates are equally  
 735 expected to form low energy gas phase ion-dipole complexes (ROOH·NO<sub>2</sub><sup>+</sup>) with bound  
 736 energies of 92 kJ mol<sup>-1</sup> in the case of methyl-peroxynitrate (Ravelo and Francisco, 2007).  
 737 Previous studies (Hansel and Wisthaler, 2000) have proposed a speculative decomposition of  
 738 the protonated PAN:



740 The same mechanism is equally indicated by later studies (Aoki et al., 2007), giving the mass  
 741 spectral signal at  $m/z = 77$ , as recorded in the case of the PAN (Figure S6). According to their  
 742 statements the other protonated PANs parent compound generated in our study (C<sub>4</sub>H<sub>7</sub>-  
 743 C(O)OONO<sub>2</sub>H<sup>+</sup>,  $m/z = 162$ ) should lead to representative ionic signals of type C<sub>4</sub>H<sub>7</sub>-  
 744 C(O)OOHH<sup>+</sup>,  $m/z = 117$ , which are indeed present in the deconvoluted mass spectra of our  
 745 analytes. Moreover, the fact that this signal is absent during the NO<sup>+</sup> ionization mode  
 746 (characterized by inferior H<sub>2</sub>O levels) may support this hypothetic decomposition of the  
 747 PANs.

748 Another likely mechanism which, unexpectedly, may lead to the same analytical signal is  
 749 reviewed by (Roberts, 1990) proposing the unimolecular decomposition of PANs to form the  
 750 corresponding C<sub>n-1</sub> alkyl nitrate. In our particular case the reaction may be written as:



752 Assuming the presence of both processes, the resulting alkyl nitrate may interfere with the  
 753 above mentioned  $m/z=117$  signal in the case of a charge transfer reaction. More likely, in the  
 754 case of a protonation process, the obtained  $m/z=118$  signal derived from the alkyl nitrate will  
 755 enhance the isobaric signal due to the <sup>13</sup>C isotopic abundance of the analyte obtained by PAN



756 decomposition. The signal of  $m/z$  118 seems indicative of the presence of a double peak  
757 which might confirm the occurrence of both processes. This fact is equally confirmed by the  
758  $I_{118}/I_{117}$  measured ratio (0.19 - 0.23 for the P2MCrN and 0.52 - 0.57 for the P3MCrN) which  
759 is significantly different from the expected  $^{13}\text{C}$  isotopic abundance for a  $\text{RC}(\text{O})\text{OOHH}^+$  type  
760 compound (0.06). This difference suggests the presence of this kind of analytical interference,  
761 more pronounced in the case of P3MCrN.

762 However the PAN decomposition path is considered to be several hundred times slower than  
763 the bond homolysis channel:



765 The recombination of  $\text{C}_4\text{H}_7\text{-C}(\text{O})\text{OO}^\cdot$  ( $m/z = 115$ ) with highly abundant  $\text{H}^+(\text{H}_2\text{O})$  and  
766  $\text{H}^+(\text{H}_2\text{O})_2$  could generate the signals at  $m/z$  133 and 151 respectively. Additionally, the high  
767 levels of  $\text{NO}_2^+$  ( $m/z = 46$ ) may favor the presence of  $\text{NO}_2^+\cdot\text{H}_2\text{O}$  ( $m/z = 64$ ) which can  
768 potentially quench the  $\text{C}_4\text{H}_7\text{-C}(\text{O})\text{OO}^\cdot$  radical to give an adduct signal at  $m/z = 179$ .

769 In order to certify the mono-nitrogen containing analytes for several ion signals in the  
770 spectrum, an analysis similar to the one performed by Inomata et al. (2013) which consists in  
771 subtraction of the isotopic effect of  $^{13}\text{C}$  by calculating  $I_{\text{even}} / I_{\text{odd}}$  ratios of an ion signal at an  
772 even  $m/z$  [M] to the adjacent ion signal at an odd  $m/z$  [M+1].

773 As described by Table 2 the normalized sensitivity for the protonated PANs is weak spanning  
774 few counts  $\text{ppb}^{-1} \text{min}^{-1}$  for all three considered PANs.

775

### 776 **3.5.2 The $\text{NO}^+$ ionization**

777 Unlike the keto-nitrates, the PANs present a low sensibility towards detection in  $\text{NO}^+$   
778 ionization mode and generally a complex chemical equilibrium in classical PTR analysis.

779 In the  $\text{NO}^+$  ionization mode, the signals corresponding to the adduct formation is barely  
780 noticed for the entire range of E/N considered. However the presence of weak signals at  $m/z =$   
781 191 and 207 for both P2MCrN and P3MCrN, are indicative of the presence of PAN  $\text{NO}^+$  and  
782 PAN  $\text{NO}_2^+$  adducts respectively.

783



#### 784 **4 Conclusions**

785 Organic nitrates play a key role in atmospheric chemistry as they act as reactive nitrogen  
786 reservoir species. The use of PTR-MS for the measurement of VOCs has expanded a lot in  
787 atmospheric research these last years but few studies have investigated the performances of  
788 this instrument for the detection of organic nitrates. These studies have shown that this  
789 technique exhibits poor performances (high fragmentation and poor sensitivity) when it is run  
790 in classical mode. In the present work, the detection of alkyl and multifunctional organic  
791 nitrates (PANs, ketonitrates, hydroxynitrates) by this technique has been studied by operating  
792 the instrument in the classical mode ( $\text{H}_3\text{O}^+$  as ionizing species) but also by testing an  
793 ionization induced by  $\text{NO}^+$ . This study has shown that a soft ionization by  $\text{NO}^+$  using low E/N  
794 ratios ( $<50$  Td) promotes the R- $\text{NO}^+$  adduct formation and minimizes the fragmentation,  
795 favoring the identification of molecular composition. In addition, the versatility of the  
796 instrument allows an easy change of the chemical ionization source, from  $\text{H}_3\text{O}^+$  to  $\text{NO}^+$  by  
797 simply replacing water vapor by dry air in the glow discharge. This is very useful for a double  
798 identification of the organic nitrates. In terms of sensitivity, the  $\text{NO}^+$  adduct ionization mode  
799 appears to be the most sensitive for the detection of hydroxy- and ketonitrates with detection  
800 limits in the range of tens ppt/min. This sensitivity is suitable for measurement of organic  
801 nitrates during lab studies but also in ambient air. The detection of alkyl nitrates and PANs  
802 with PTR-MS is less sensitive, with detection limits in the range of hundreds ppt/min,  
803 whatever the ionization source used. For these two classes of nitrates, accumulations over  
804 longer periods will be necessary for measurements in ambient air.

805 A crucial aspect to be taken into account in further studies for lab and field measurements  
806 deployment of the method will be the effect of the humidity of the sampled air. In addition,  
807 longer acquisition time, elimination of interfering ionization paths by selective ionization  
808 sources and softer ionization sources could improve the technique's performances.

809

#### 810 **5 Acknowledgements**

811 This work was supported by the French National Agency for Research (Project ONCEM-  
812 ANR-12-BS06-0017-01), by the European Community within the seventh Framework  
813 Program, section "Support for Research Infrastructure-Integrated Infrastructure Initiative":



814 EUROCHAMP-2 (RII3-CT-2009-228335) and by the Région Ile de France. The authors also  
815 thank Fraiser Reich and Kore Company for their advices in the use of the PTR-MS.

816

## 817 **6 References**

818 Amadei, G. and Ross, B. M.: The reactions of a series of terpenoids with  $\text{H}_3\text{O}^+$ ,  $\text{NO}^+$  and  $\text{O}_2^+$   
819 studied using selected ion flow tube mass spectrometry, *Rapid Commun. Mass Spectrom.*, 25,  
820 162-168, 2011.

821 Aoki, N., Inomata, S., and Tanimoto, H.: Detection of  $\text{C}_1$ - $\text{C}_5$  alkyl nitrates by proton transfer  
822 reaction time-of-flight mass spectrometry, *Int. J. Mass Spectrom.*, 263, 12-21, 2007.

823 Arey, J., Aschmann, S. M., Kwok, E. S. C., and Atkinson, R.: Alkyl Nitrate, Hydroxyalkyl  
824 Nitrate, and Hydroxycarbonyl Formation from the  $\text{NO}_x$  - Air Photooxidations of  $\text{C}_5$ - $\text{C}_8$  n-  
825 Alkanes, *Journal of Physical Chemistry A*, 105, 1020-1027, 2001.

826 Atkinson, R.: Atmospheric chemistry of VOCs and  $\text{NO}_x$ , *Atmos. Environ.*, 34, 2063-2101,  
827 2000.

828 Atlas, E.: Evidence for  $\geq\text{C}_3$  alkyl nitrates in rural and remote atmospheres, *Nature*, 331, 426-  
829 428, 1988.

830 Barber, S., Blake, R. S., White, I. R., Monks, P. S., Reich, F., Mullock, S., and Ellis, A. M.:  
831 Increased Sensitivity in Proton Transfer Reaction Mass Spectrometry by Incorporation of a  
832 Radio Frequency Ion Funnel, *Anal. Chem.*, 84, 5387-5391, 2012.

833 Barnes, I., Bastian, V., Becker, K. H., and Tong, Z.: Kinetics and products of the reactions of  
834 nitrate radical with monoalkenes, dialkenes, and monoterpenes, *The Journal of Physical  
835 Chemistry*, 94, 2413-2419, 1990.

836 Bates, K. H., Crouse, J. D., St. Clair, J. M., Bennett, N. B., Nguyen, T. B., Seinfeld, J. H.,  
837 Stoltz, B. M., and Wennberg, P. O.: Gas phase production and loss of isoprene epoxydiols,  
838 *Journal of Physical Chemistry A*, 118, 1237-1246, 2014.

839 Baughman, T. W., Sworen, J. C., and Wagener, K. B.: The facile preparation of alkenyl  
840 metathesis synthons, *Tetrahedron*, 60, 10943-10948, 2004.

841 Beaver, M. R., St. Clair, J. M., Paulot, F., Spencer, K. M., Crouse, J. D., Lafranchi, B. W.,  
842 Min, K. E., Pusede, S. E., Wooldridge, P. J., Schade, G. W., Park, C., Cohen, R. C., and  
843 Wennberg, P. O.: Importance of biogenic precursors to the budget of organic nitrates:  
844 Observations of multifunctional organic nitrates by CIMS and TD-LIF during BEARPEX  
845 2009, *Atmos. Chem. Phys.*, 12, 5773-5785, 2012.

846 Blake, N. J., Blake, D. R., Wingenter, O. W., Sive, B. C., Kang, C. H., Thornton, D. C.,  
847 Bandy, A. R., Atlas, E., Flocke, F., Harris, J. M., and Rowland, F. S.: Aircraft measurements  
848 of the latitudinal, vertical, and seasonal variations of NMHCs, methyl nitrate, methyl halides,  
849 and DMS during the First Aerosol Characterization Experiment (ACE 1), *Journal of  
850 Geophysical Research: Atmospheres*, 104, 21803-21817, 1999.

851 Blake, R. S., Monks, P. S., and Ellis, A. M.: Proton-Transfer Reaction Mass Spectrometry,  
852 *Chem. Rev.*, 109, 861-896, 2009.



- 853 Browne, E. C., Min, K. E., Wooldridge, P. J., Apel, E., Blake, D. R., Brune, W. H., Cantrell,  
854 C. A., Cubison, M. J., Diskin, G. S., Jimenez, J. L., Weinheimer, A. J., Wennberg, P. O.,  
855 Wisthaler, A., and Cohen, R. C.: Observations of total RONO<sub>2</sub> over the boreal forest: NO<sub>x</sub>  
856 sinks and HNO<sub>3</sub> sources, *Atmos. Chem. Phys.*, 13, 4543-4562, 2013.
- 857 Buhr, M. P., Parrish, D. D., Norton, R. B., Fehsenfeld, F. C., Sievers, R. E., and Roberts, J.  
858 M.: Contribution of organic nitrates to the total reactive nitrogen budget at a rural eastern U.S.  
859 site, *Journal of Geophysical Research: Atmospheres*, 95, 9809-9816, 1990.
- 860 Cacace, F. and de Petris, G.: Mass spectrometric study of simple main group molecules and  
861 ions important in atmospheric processes, *Int. J. Mass Spectrom.*, 194, 1-10, 2000.
- 862 Cacace, F., de Petris, G., and Pepi, F.: Gas-phase NO<sup>+</sup> affinities, *Proceedings of the National*  
863 *Academy of Sciences of the United States of America*, 94, 3507-3512, 1997.
- 864 Castedo, L., Marcos, C. F., Monteagudo, M., and Tojo, G.: New One-Pot Synthesis of Alkyl  
865 Nitrates from Alcohols, *Synthetic Communications*, 22, 677-681, 1992.
- 866 Curci, G., Beekmann, M., Vautard, R., Smiattek, G., Steinbrecher, R., Theloke, J., and  
867 Friedrich, R.: Modelling study of the impact of isoprene and terpene biogenic emissions on  
868 European ozone levels, *Atmos. Environ.*, 43, 1444-1455, 2009.
- 869 D'Anna, B., Wisthaler, A., Andreasen, Ø., Hansel, A., Hjorth, J., Jensen, N. R., Nielsen, C. J.,  
870 Stenstrøm, Y., and Viidanoja, J.: Atmospheric Chemistry of C<sub>3</sub>-C<sub>6</sub>  
871 Cycloalkanecarbaldehydes, *The Journal of Physical Chemistry A*, 109, 5104-5118, 2005.
- 872 Day, D. A., Wooldridge, P. J., Dillon, M. B., Thornton, J. A., and Cohen, R. C.: A thermal  
873 dissociation laser-induced fluorescence instrument for in situ detection of NO<sub>2</sub>, peroxy  
874 nitrates, alkyl nitrates, and HNO<sub>3</sub>, *J. Geophys. Res.-Atmos.*, 107, 5-6, 2002.
- 875 de Gouw, J. and Warneke, C.: Measurements of volatile organic compounds in the earths  
876 atmosphere using proton-transfer-reaction mass spectrometry, *Mass Spectrom. Rev.*, 26, 223-  
877 257, 2007.
- 878 de Gouw, J., Warneke, C., Karl, T., Eerdeken, G., van der Veen, C., and Fall, R.: Sensitivity  
879 and specificity of atmospheric trace gas detection by proton-transfer-reaction mass  
880 spectrometry, *Int. J. Mass Spectrom.*, 223-224, 365-382, 2003.
- 881 De Laeter, J. R., Böhlke, J. K., De Bièvre, P., Hidaka, H., Peiser, H. S., Rosman, K. J. R., and  
882 Taylor, P. D. P.: Atomic weights of the elements: Review 2000 (IUPAC Technical Report),  
883 *Pure and Applied Chemistry*, 75, 683-800, 2003.
- 884 Diskin, A. M., Wang, T., Smith, D., and Španěl, P.: A selected ion flow tube (SIFT), study of  
885 the reactions of H<sub>3</sub>O<sup>+</sup>, NO<sup>+</sup> and O<sub>2</sub><sup>+</sup> ions with a series of alkenes; in support of SIFT-MS, *Int.*  
886 *J. Mass Spectrom.*, 218, 87-101, 2002.
- 887 Doussin, J. F., Picquet-Varrault, B., Durand-Jolibois, R., Loirat, H., and Carlier, P.: A visible  
888 and FTIR spectrometric study of the nighttime chemistry of acetaldehyde and PAN under  
889 simulated atmospheric conditions, *Journal of Photochemistry and Photobiology A: Chemistry*,  
890 157, 283-293, 2003.
- 891 Fischer, R., Weller, R., Jacobi, H.-W., and Ballschmiter, K.: Levels and pattern of volatile  
892 organic nitrates and halocarbons in the air at Neumayer Station (70°S), Antarctic,  
893 *Chemosphere*, 48, 981-992, 2002.



- 894 Fischer, R. G., Kastler, J., and Ballschmiter, K.: Levels and pattern of alkyl nitrates,  
895 multifunctional alkyl nitrates, and halocarbons in the air over the Atlantic Ocean, *Journal of*  
896 *Geophysical Research: Atmospheres*, 105, 14473-14494, 2000.
- 897 Flocke, F., Volz-Thomas, A., and Kley, D.: Measurements of alkyl nitrates in rural and  
898 polluted air masses, *Atmospheric Environment Part A, General Topics*, 25, 1951-1960, 1991.
- 899 Flocke, F. M., Weinheimer, A. J., Swanson, A. L., Roberts, J. M., Schmitt, R., and Shertz, S.:  
900 On the measurement of PANs by gas chromatography and electron capture detection, *J.*  
901 *Atmos. Chem.*, 52, 19-43, 2005.
- 902 Francisco, M. A. and Krylowski, J.: Chemistry of Organic Nitrates: Thermal Chemistry of  
903 Linear and Branched Organic Nitrates, *Industrial & Engineering Chemistry Research*, 44,  
904 5439-5446, 2005.
- 905 Fukui, Y. and Doskey, P. V.: A Measurement Technique for Organic Nitrates and  
906 Halocarbons in Ambient Air, *Journal of High Resolution Chromatography*, 21, 201-208,  
907 1998.
- 908 Gaffney, J. S., Marley, N. A., Steele, H. D., Drayton, P. J., and Hubbe, J. M.: Aircraft  
909 Measurements of Nitrogen Dioxide and Peroxyacyl Nitrates Using Luminol  
910 Chemiluminescence with Fast Capillary Gas Chromatography, *Environ. Sci. Technol.*, 33,  
911 3285-3289, 1999.
- 912 Goebbert, D. and Wentold, P.: Water dimer proton affinity from the kinetic method:  
913 dissociation energy of the water dimer, *European Journal of Mass Spectrometry*, 10, 837-846,  
914 2004.
- 915 Grosjean, D. and Harrison, J.: Peroxyacetyl Nitrate - Comparison of Alkaline-Hydrolysis and  
916 Chemi-Luminescence Methods, *Environ. Sci. Technol.*, 19, 749-752, 1985.
- 917 Hansel, A. and Wisthaler, A.: A method for real-time detection of PAN, PPN and MPAN in  
918 ambient air, *Geophys. Res. Lett.*, 27, 895-898, 2000.
- 919 Hanst, P. L.: Mechanism of Peroxyacetyl Nitrate Formation, *Journal of the Air Pollution*  
920 *Control Association*, 21, 269-271, 1971.
- 921 Hao, C., Shepson, B., Drummond, J. W., and Muthuramu, K.: Gas chromatographic detector  
922 for selective and sensitive detection of atmospheric organic nitrates, *Anal. Chem.*, 66, 3737-  
923 3743, 1994.
- 924 Harrison, A. G.: Chemical Ionization in Mass Spectrometry\*. In: *Encyclopedia of*  
925 *Spectroscopy and Spectrometry (Second Edition)*, Lindon, J. C. (Ed.), Academic Press,  
926 Oxford, 1999.
- 927 Hewitt, C. N., Hayward, S., and Tani, A.: The application of proton transfer reaction-mass  
928 spectrometry (PTR-MS) to the monitoring and analysis of volatile organic compounds in the  
929 atmosphere, *J. Environ. Monit.*, 5, 1-7, 2003.
- 930 Horowitz, L. W., Fiore, A. M., Milly, G. P., Cohen, R. C., Perring, A., Wooldridge, P. J.,  
931 Hess, P. G., Emmons, L. K., and Lamarque, J. F.: Observational constraints on the chemistry  
932 of isoprene nitrates over the eastern United States, *Journal of Geophysical Research*  
933 *Atmospheres*, 112, 2007.
- 934 Huey, L. G.: Measurement of trace atmospheric species by chemical ionization mass  
935 spectrometry: Speciation of reactive nitrogen and future directions, *Mass Spectrom. Rev.*, 26,  
936 166-184, 2007.



- 937 Iachetta, L., Malek, L., and Ross, B. M.: The reactions of  $\text{H}_3\text{O}^+$ ,  $\text{NO}^+$  and  $\text{O}_2^+$  with several  
938 flavourant esters studied using selected ion flow tube mass spectrometry, *Rapid Commun.*  
939 *Mass Spectrom.*, 24, 815-822, 2010.
- 940 Inomata, S., Tanimoto, H., Fujitani, Y., Sekimoto, K., Sato, K., Fushimi, A., Yamada, H.,  
941 Hori, S., Kumazawa, Y., Shimono, A., and Hikida, T.: On-line measurements of gaseous  
942 nitro-organic compounds in diesel vehicle exhaust by proton-transfer-reaction mass  
943 spectrometry, *Atmos. Environ.*, 73, 195-203, 2013.
- 944 Jacobs, M. I., Burke, W. J., and Elrod, M. J.: Kinetics of the reactions of isoprene-derived  
945 hydroxynitrates: gas phase epoxide formation and solution phase hydrolysis, *Atmos. Chem.*  
946 *Phys.*, 14, 8933-8946, 2014.
- 947 Kames, J., Schurath, U., Flocke, F., and Volz-Thomas, A.: Preparation of organic nitrates  
948 from alcohols and  $\text{N}_2\text{O}_5$  for species identification in atmospheric samples, *J. Atmos. Chem.*,  
949 16, 349-359, 1993.
- 950 Karl, T., Hansel, A., Cappellin, L., Kaser, L., Herdinger-Blatt, I., and Jud, W.: Selective  
951 measurements of isoprene and 2-methyl-3-buten-2-ol based on  $\text{NO}^+$  ionization mass  
952 spectrometry, *Atmos. Chem. Phys.*, 12, 11877-11884, 2012.
- 953 Kastler, J. and Ballschmiter, K.: Identification of alkyl dinitrates in ambient air of Central  
954 Europe, *Fresenius' Journal of Analytical Chemistry*, 363, 1-4, 1999.
- 955 Knighton, W. B., Fortner, E. C., Herndon, S. C., Wood, E. C., and Miake-Lye, R. C.:  
956 Adaptation of a proton transfer reaction mass spectrometer instrument to employ  $\text{NO}^+$  as  
957 reagent ion for the detection of 1,3-butadiene in the ambient atmosphere, *Rapid Commun.*  
958 *Mass Spectrom.*, 23, 3301-3308, 2009.
- 959 Kriemler, P. and Buttrill, S. E.: Positive and negative ion-molecule reactions and the proton  
960 affinity of ethyl nitrate, *Journal of the American Chemical Society*, 92, 1123-1128, 1970.
- 961 Lee, B. H., Lopez-Hilfiker, F. D., Mohr, C., Kurtén, T., Worsnop, D. R., and Thornton, J. A.:  
962 An iodide-adduct high-resolution time-of-flight chemical-ionization mass spectrometer:  
963 Application to atmospheric inorganic and organic compounds, *Environmental Science and*  
964 *Technology*, 48, 6309-6317, 2014.
- 965 Lee, T. J. and Rice, J. E.: Proton affinity of methyl nitrate: less than proton affinity of nitric  
966 acid, *Journal of the American Chemical Society*, 114, 8247-8256, 1992.
- 967 Luxenhofer, O. and Ballschmiter, K.: C4-C14-alkyl nitrates as organic trace compounds in  
968 air, *Fresenius' Journal of Analytical Chemistry*, 350, 395-402, 1994.
- 969 Luxenhofer, O., Schneider, E., and Ballschmiter, K.: Separation, detection and occurrence of  
970 (C2-C8)-alkyl- and phenyl-alkyl nitrates as trace compounds in clean and polluted air,  
971 *Fresenius' Journal of Analytical Chemistry*, 350, 384-394, 1994.
- 972 Madronich, S. and Calvert, J. G.: Permutation reactions of organic peroxy radicals in the  
973 troposphere, *Journal of Geophysical Research*, 95, 5697-5715, 1990.
- 974 Mills, G. P., Hiatt-Gipson, G. D., Bew, S. P., and Reeves, C. E.: Measurement of isoprene  
975 nitrates by GCMS, *Atmos. Meas. Tech. Discuss.*, 2016, 1-24, 2016.
- 976 Mochalski, P., Unterkofler, K., Španěl, P., Smith, D., and Amann, A.: Product ion  
977 distributions for the reactions of  $\text{NO}^+$  with some physiologically significant aldehydes  
978 obtained using a SRI-TOF-MS instrument, *Int. J. Mass Spectrom.*, 363, 23-31, 2014.



- 979 Müller, M., Graus, M., Wisthaler, A., Hansel, A., Metzger, A., Dommen, J., and  
980 Baltensperger, U.: Analysis of high mass resolution PTR-TOF mass spectra from 1,3,5-  
981 trimethylbenzene (TMB) environmental chamber experiments, *Atmos. Chem. Phys.*, 12, 829-  
982 843, 2012.
- 983 Muthuramu, K., Shepson, P. B., and O'Brien, J. M.: Preparation, analysis, and atmospheric  
984 production of multifunctional organic nitrates, *Environ. Sci. Technol.*, 27, 1117-1124, 1993.
- 985 O'Brien, J. M., Shepson, P. B., Muthuramu, K., Hao, C., Niki, H., Hastie, D. R., Taylor, R.,  
986 and Roussel, P. B.: Measurements of alkyl and multifunctional organic nitrates at a rural site  
987 in Ontario, *Journal of Geophysical Research: Atmospheres*, 100, 22795-22804, 1995.
- 988 Paul, D., Furgeson, A., and Osthoff, H. D.: Measurements of total peroxy and alkyl nitrate  
989 abundances in laboratory-generated gas samples by thermal dissociation cavity ring-down  
990 spectroscopy, *Review of Scientific Instruments*, 80, 2009.
- 991 Perraud, V., Bruns, E. A., Ezell, M. J., Johnson, S. N., Greaves, J., and Finlayson-Pitts, B. J.:  
992 Identification of Organic Nitrates in the NO<sub>3</sub> Radical Initiated Oxidation of alpha-Pinene by  
993 Atmospheric Pressure Chemical Ionization Mass Spectrometry, *Environ. Sci. Technol.*, 44,  
994 5887-5893, 2010.
- 995 Perring, A. E., Bertram, T. H., Farmer, D. K., Wooldridge, P. J., Dibb, J., Blake, N. J., Blake,  
996 D. R., Singh, H. B., Fuelberg, H., Diskin, G., Sachse, G., and Cohen, R. C.: The production  
997 and persistence of ΣRONO<sub>2</sub> in the Mexico City plume, *Atmos. Chem. Phys.*, 10, 7215-7229,  
998 2010.
- 999 Ravelo, R. M. and Francisco, J. S.: Proton Affinity of Methyl Peroxynitrate, *The Journal of*  
1000 *Physical Chemistry A*, 112, 1981-1985, 2007.
- 1001 Rimetz-Planchon, J., Dhooghe, F., Schoon, N., Vanhaecke, F., and Amelynck, C.: Chemical  
1002 ionization by [NO]<sup>+</sup> and subsequent collision-induced dissociation for the selective on-line  
1003 detection of monoterpenes and linalool, *Rapid communications in mass spectrometry : RCM*,  
1004 25, 647-654, 2011.
- 1005 Roberts, J. M.: The atmospheric chemistry of organic nitrates, *Atmospheric Environment*.  
1006 Part A. General Topics, 24, 243-287, 1990.
- 1007 Roberts, J. M., Flocke, F., Stroud, C. A., Hereid, D., Williams, E., Fehsenfeld, F., Brune, W.,  
1008 Martinez, M., and Harder, H.: Ground-based measurements of peroxy-carboxylic nitric  
1009 anhydrides (PANs) during the 1999 Southern Oxidants Study Nashville Intensive, *Journal of*  
1010 *Geophysical Research: Atmospheres*, 107, 2002.
- 1011 Rollins, A. W., Fry, J. L., Hunter, J. F., Kroll, J. H., Worsnop, D. R., Singaram, S. W., and  
1012 Cohen, R. C.: Elemental analysis of aerosol organic nitrates with electron ionization high-  
1013 resolution mass spectrometry, *Atmos. Meas. Tech.*, 3, 301-310, 2010.
- 1014 Sadanaga, Y., Takaji, R., Ishiyama, A., Nakajima, K., Matsuki, A., and Bandow, H.: Thermal  
1015 dissociation cavity attenuated phase shift spectroscopy for continuous measurement of total  
1016 peroxy and organic nitrates in the clean atmosphere, *Review of Scientific Instruments*, 87,  
1017 074102, 2016.
- 1018 Schoon, N., Amelynck, C., Debie, E., Bultinck, P., and Arijs, E.: A selected ion flow tube  
1019 study of the reactions of H<sub>3</sub>O<sup>+</sup>, NO<sup>+</sup> and O<sub>2</sub><sup>+</sup> with a series of C<sub>5</sub>, C<sub>6</sub> and C<sub>8</sub> unsaturated  
1020 biogenic alcohols, *Int. J. Mass Spectrom.*, 263, 127-136, 2007.





- 1021 Slusher, D. L., Huey, L. G., Tanner, D. J., Flocke, F. M., and Roberts, J. M.: A thermal  
1022 dissociation–chemical ionization mass spectrometry (TD-CIMS) technique for the  
1023 simultaneous measurement of peroxyacyl nitrates and dinitrogen pentoxide, *Journal of*  
1024 *Geophysical Research: Atmospheres*, 109, D19315, 2004.
- 1025 Smith, D., Sovová, K., and Španěl, P.: A selected ion flow tube study of the reactions of  
1026  $\text{H}_3\text{O}^+$ ,  $\text{NO}^+$  and  $\text{O}_2^{+\bullet}$  with seven isomers of hexanol in support of SIFT-MS, *Int. J. Mass*  
1027 *Spectrom.*, 319–320, 25–30, 2012.
- 1028 Smith, D. and Španěl, P.: Selected ion flow tube mass spectrometry (SIFT-MS) for on-line  
1029 trace gas analysis, *Mass Spectrom. Rev.*, 24, 661–700, 2005.
- 1030 Smith, D., Wang, T., and Španěl, P.: Analysis of ketones by selected ion flow tube mass  
1031 spectrometry, *Rapid Commun. Mass Spectrom.*, 17, 2655–2660, 2003.
- 1032 Smith, G.: Comparative Analysis of Tekmar 3000 and 3100 Purge and Trap Sample  
1033 Concentrators: Performance Evaluation Between Electroform Nickel and Silcosteel-coated  
1034 Sample Pathways, Tekmar, Mason, OH, <http://www.tekmar.com> pp., 2003.
- 1035 Španěl, P. and Smith, D.: SIFT studies of the reactions of  $\text{H}_3\text{O}^+$ ,  $\text{NO}^+$  and  $\text{O}_2^+$  with a series of  
1036 alcohols, *International Journal of Mass Spectrometry and Ion Processes*, 167–168, 375–388,  
1037 1997.
- 1038 Španěl, P. and Smith, D.: Selected ion flow tube studies of the reactions of  $\text{H}_3\text{O}^+$ ,  $\text{NO}^+$ , and  
1039  $\text{O}_2^+$  with several aromatic and aliphatic hydrocarbons, *Int. J. Mass Spectrom.*, 181, 1–10,  
1040 1998.
- 1041 Tanimoto, H., Hirokawa, J., Kajii, Y., and Akimoto, H.: A new measurement technique of  
1042 peroxyacetyl nitrate at parts per trillion by volume levels: Gas chromatography/negative ion  
1043 chemical ionization mass spectrometry, *Journal of Geophysical Research: Atmospheres*, 104,  
1044 21343–21354, 1999.
- 1045 Teng, A. P., Crouse, J. D., Lee, L., St. Clair, J. M., Cohen, R. C., and Wennberg, P. O.:  
1046 Hydroxy nitrate production in the OH-initiated oxidation of alkenes, *Atmos. Chem. Phys.*  
1047 *Discuss.*, 14, 6721–6757, 2014.
- 1048 Tuazon, E. C., Alvarado, A., Aschmann, S. M., Atkinson, R., and Arey, J.: Products of the  
1049 Gas-Phase Reactions of 1,3-Butadiene with OH and  $\text{NO}_3$  Radicals, *Environ. Sci. Technol.*, 33,  
1050 3586–3595, 1999.
- 1051 Tureček, F.: Proton affinity of peroxyacetyl nitrate. A computational study of topical proton  
1052 affinities, *Journal of Mass Spectrometry*, 35, 1351–1359, 2000.
- 1053 Wang, T., Španěl, P., and Smith, D.: A selected ion flow tube study of the reactions of  $\text{H}_3\text{O}^+$ ,  
1054  $\text{NO}^+$  and  $\text{O}_2^{+\bullet}$  with some phenols, phenyl alcohols and cyclic carbonyl compounds in support  
1055 of SIFT-MS and PTR-MS, *Int. J. Mass Spectrom.*, 239, 139–146, 2004.
- 1056 Winer, A. M., Peters, J. W., Smith, J. P., and Pitts, J. N.: Response of commercial  
1057 chemiluminescent nitric oxide-nitrogen dioxide analyzers to other nitrogen-containing  
1058 compounds, *Environ. Sci. Technol.*, 8, 1118–1121, 1974.
- 1059 Xiong, F., McAvey, K. M., Pratt, K. A., Groff, C. J., Hostetler, M. A., Lipton, M. A., Starn,  
1060 T. K., Seeley, J. V., Bertman, S. B., Teng, A. P., Crouse, J. D., Nguyen, T. B., Wennberg, P.  
1061 O., Misztal, P. K., Goldstein, A. H., Guenther, A. B., Koss, A. R., Olson, K. F., De Gouw, J.  
1062 A., Baumann, K., Edgerton, E. S., Feiner, P. A., Zhang, L., Miller, D. O., Brune, W. H., and



1063 Shepson, P. B.: Observation of isoprene hydroxynitrates in the southeastern United States and  
1064 implications for the fate of NO<sub>x</sub>, Atmos. Chem. Phys., 15, 11257-11272, 2015.  
1065



1 *Table 1 Summarized analytical approaches into the organic nitrate analysis*

Type of study	Analytes	DL / time or normalized sensitivity	Ionizing species	Experimental setup	Study
Synthesis	PAN	< 40 ppb	O <sub>3</sub> +NO KOH / O <sub>3</sub> +NO	CL NO <sub>x</sub> IC KOH / CL NO <sub>x</sub>	Winer et al. (1974) Grosjean and Harrison (1985)
Field campaign	PAN	10-80 ppt / 1 min	luminol	CL NO <sub>2</sub>	Gaffney et al. (1999)
Synthesis	C <sub>3</sub> -C <sub>5</sub> alkyl nitrates C <sub>2</sub> -C <sub>4</sub> hydroxy nitrates C <sub>2</sub> -C <sub>4</sub> dinitrates		e <sup>-</sup> / luminol	GC-ECD –CL NO <sub>2</sub>	Hao et al. (1994)
Laboratory / Field campaign	ΣAN, ΣPN	30-90 ppt	-	TD-LIF	Day et al. (2002)
Field campaign	ΣAN, ΣPN	30-90 ppt	-	TD-LIF	Perring et al. (2010)
Field campaign	C <sub>3</sub> -C <sub>5</sub> alkyl nitrates	10 ppt	e <sup>-</sup> e <sup>-th</sup>	GC-ECD GC-NICI-MS	Atlas (1988)
Field campaign	C <sub>2</sub> -C <sub>3</sub> Alkyl nitrates PAN, PPN,	10 ppt	e <sup>-</sup>	GC-ECD	Fukui and Doskey (1998)
Synthesis; cis-2-butene+OH (NO)	Alkyl nitrates α, β -hydroxynitrates, dinitrates	-	e <sup>-</sup>	GC-ECD	Muthuramu et al. (1993)
Peroxyalkyl +NO <sub>2</sub>	PAN, PPN, PIBN, MPAN, APAN, PnBN, PBZN	2 ppt	e <sup>-</sup>	GC-ECD	Flocke et al. (2005)
Field campaign	C <sub>4</sub> -C <sub>14</sub> alkyl nitrates (C <sub>2</sub> -C <sub>8</sub> )-alkyl- and phenyl-alkyl-nitrates	1 ppt	e <sup>-</sup>	GC-ECD GC-El-MS	Luxenhofer and Ballschmitter (1994) Luxenhofer et al. (1994)



<b>Field campaign</b>	C <sub>6</sub> -C <sub>13</sub> alkyl nitrates C <sub>3</sub> -C <sub>6</sub> dinitrates C <sub>2</sub> -C <sub>6</sub> hydroxynitrates	e <sup>-</sup>	HPLC / GC-ECD GC-EI-MS	Fischer et al. (2000) Kastler and Ballschmiter (1999)
<b>Field campaign</b>	PAN, PPN, MPAN, 15 ppt / 10 min	e <sup>-</sup>	GC-ECD	Tanimoto et al. (1999)
<b>Synthesis; alcohols+N<sub>2</sub>O<sub>5</sub></b>	C <sub>1</sub> -C <sub>8</sub> alkyl nitrates, ketonitrates, hydroxynitrates, dinitrates	e <sup>-</sup>	GC-ECD GC-NO <sub>y</sub> CI-MS	Kames et al. (1993)
<b>NO<sub>3</sub> + α-pinene</b>	Carbonyl hydroxi-nitrates or PANs	H <sup>+</sup> (MeOH)	APCI-MS	Perraud et al. (2010)
<b>Peroxyacetyl +NO<sub>2</sub></b>	PAN, PPN, MPAN 10 ppt /15s	I <sup>-</sup>	TD-CIMS	Slusher et al. (2004) Huey (2007)
<b>C<sub>2</sub>-C<sub>8</sub> alkenes + OH (O<sub>2</sub>, NO)</b>	β -hydroxy-nitrates 19-50 counts/ppb	CF <sub>3</sub> O <sup>-</sup>	ToF CIMS MS-MS CIMS	Teng et al. (2014)
<b>Field campaign</b>	PAN, PPN, MPAN, 25 counts/ppb	O <sub>2</sub> <sup>+</sup> , H <sub>3</sub> O <sup>+</sup> , (H <sub>2</sub> O) <sub>2</sub> H <sup>+</sup> H <sub>3</sub> O <sup>+</sup>	SIFDT* PTRMS	Hansel and Wisthaler (2000)
<b>Synthesis</b>	C <sub>1</sub> -C <sub>5</sub> alkyl nitrates 15 <sup>†</sup> counts/ppb	H <sub>3</sub> O <sup>+</sup>	PTRMS	Aoki et al. (2007)
<b>C<sub>3</sub>-C<sub>6</sub> Cycloalkanecarbaldehydes</b>	nitroperoxycarbonyl cycloalkyl nitrates counts/ppb	H <sub>3</sub> O <sup>+</sup> H <sub>3</sub> O <sup>+</sup> (H <sub>2</sub> O) <sub>h</sub>	PTRMS	D'Anna et al. (2005)

1 \* Selected Ion Flow Drift Tube; † as specific alkyl (-R<sup>+</sup>) fragment

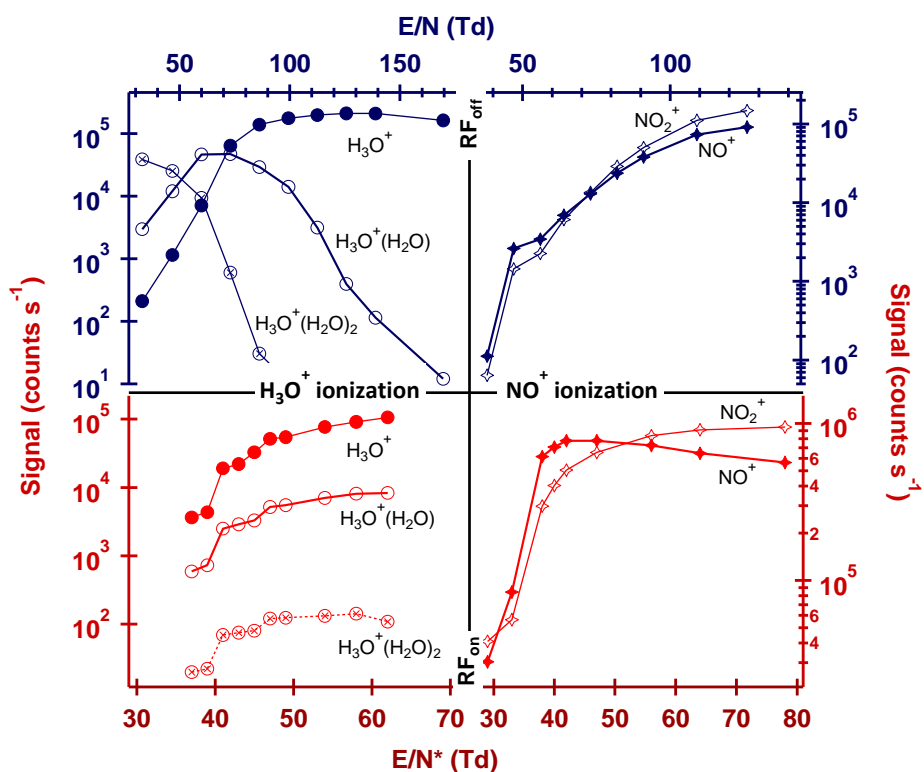
2 PAN = peroxyacetyl nitrate; PPN =peroxypropionyl nitrate; PiBN = peroxyisobutyryl nitrate; MPAN = peroxyethacetyl nitrate; APAN = peroxyacetyl nitrate; PnBN = peroxybutyryl nitrate; PBzN = peroxybenzoyl nitrate



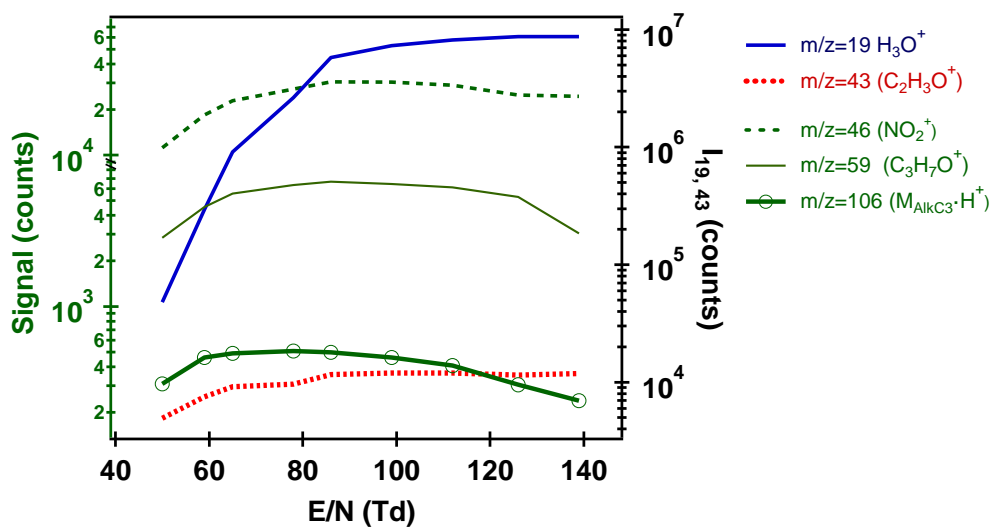
Table 2 Organic nitrates normalized sensitivity as a function of the ionization mode

Compound	MW (g mol <sup>-1</sup> )	H <sub>3</sub> O <sup>+</sup> ionization			NO <sup>+</sup> ionization		
		Signal (m/z)	Sensitivity (ncpm) ppbv <sup>-1</sup>	E/N (Td)	Signal (m/z)	Sensitivity (ncpm) ppbv <sup>-1</sup>	E/N (Td)
AlkC3 propyl nitrate	105	43	35	70	104	1.1	34*
		59	18.8		135	48.8	
		106	2				
AlkC4 isobutyl nitrate	119	57	43.4	70	118	8.3	34*
		73	23		149	78.9	
		120	2				
KnC3 nitroxyacetone	119	75	45.4 – 88.4	73 – 75	149	320 - 331	45*
		120	119 – 144	73 – 75			
		137	127	48*			
KnC5 3-nitroxy-3-methyl-2- butanone	147	103	38.3	74	177	249 - 265	39*
		148	8	74			
		165	538	48*			
PAN	121	122	7.7	90	151	weak	
1OH3C3	121	104	0.2	62	120	22.8	34*
1-hydroxy-3-nitroxy- propane		120	0.2		151	268	
		122	2		167	10.2	
		139	52.6				
		140	38				

\* Without taking into account the RF contribution



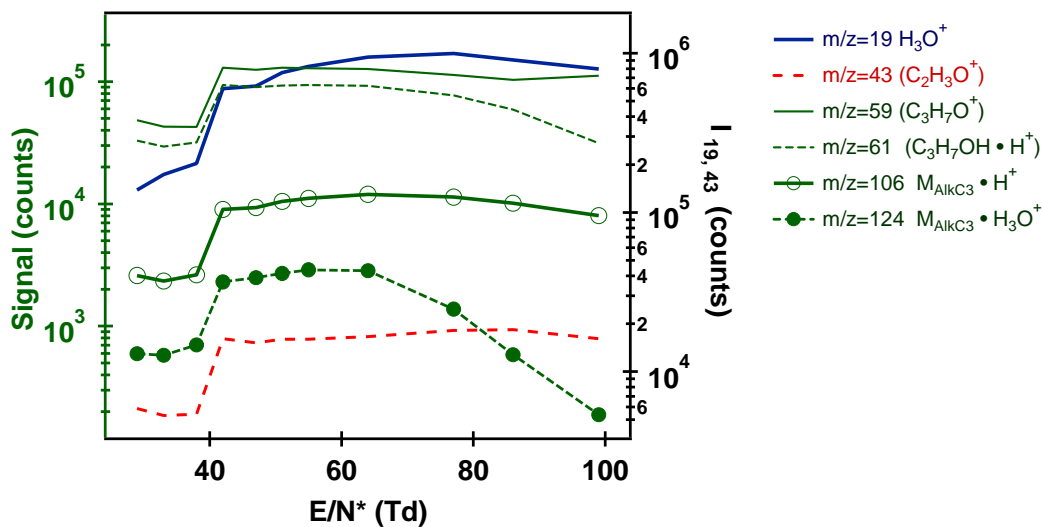
1  
 2 Figure 1. Typical ionizing species distribution as a function of the E/N ratio, in the two  
 3 ionization modes with RF mode on and off. When the RF mode is on, E/N\* ratio were  
 4 calculated taking into account only the contribution of the dc electric field while the  
 5 additional input of the ac electric field remains difficult to estimate.



1

2 Figure 2. The E/N ratio influence over the AlkC3 identification for several representative  
3 signals as recorded in absence of a RF funnel (left axis). The H<sub>3</sub>O<sup>+</sup> ion is equally illustrated in  
4 order to point the water cluster ions distribution influence, while the common signal at  
5 m/z=43 is a fragmentation mark (right axis).

6

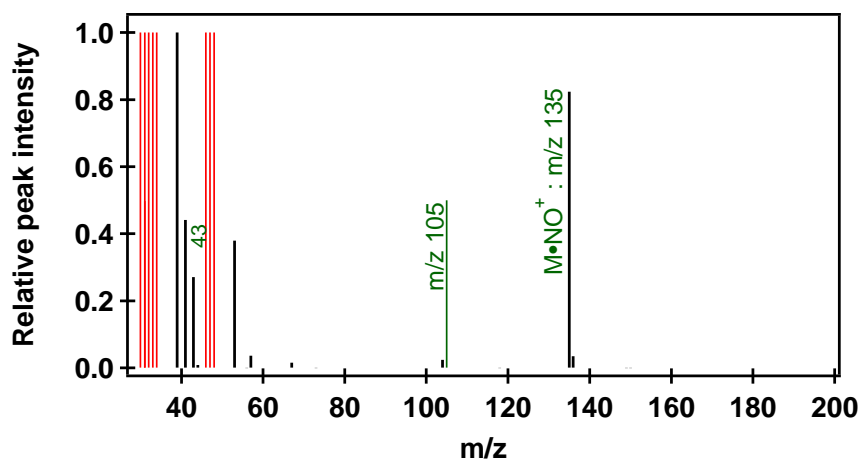


1

2 Figure 3. The E/N ratio influence over the AlkC3 identification for several representative  
 3 signals as recorded with the RF mode (left axis). The H<sub>3</sub>O<sup>+</sup> ion is equally illustrated in order  
 4 to point the water cluster ions distribution influence, while the common signal at m/z=43 is a  
 5 fragmentation mark (right axis).

6

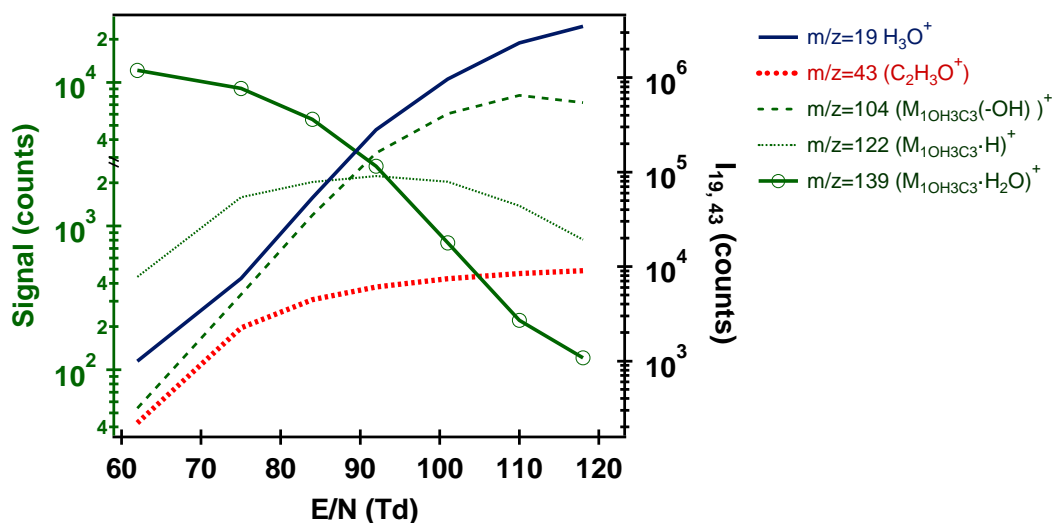




1

2 Figure 4. Recorded mass spectrum of AlkC3 (black bars) at the lowest extent of  
3 fragmentation ( $E/N^* = 34$  Td) in the  $\text{NO}^+$  ionization mode. The green thin line represents the  
4 expected molecular ion of the analyte and the intense signals depicted by the red thin bars  
5 represent the ionizing analytes at  $m/z = 30$  ( $\text{NO}^+$ ) and 46 ( $\text{NO}_2^+$ ) and their isotopic abundance  
6 signals at  $m/z = 31$  and 47, 48 respectively.

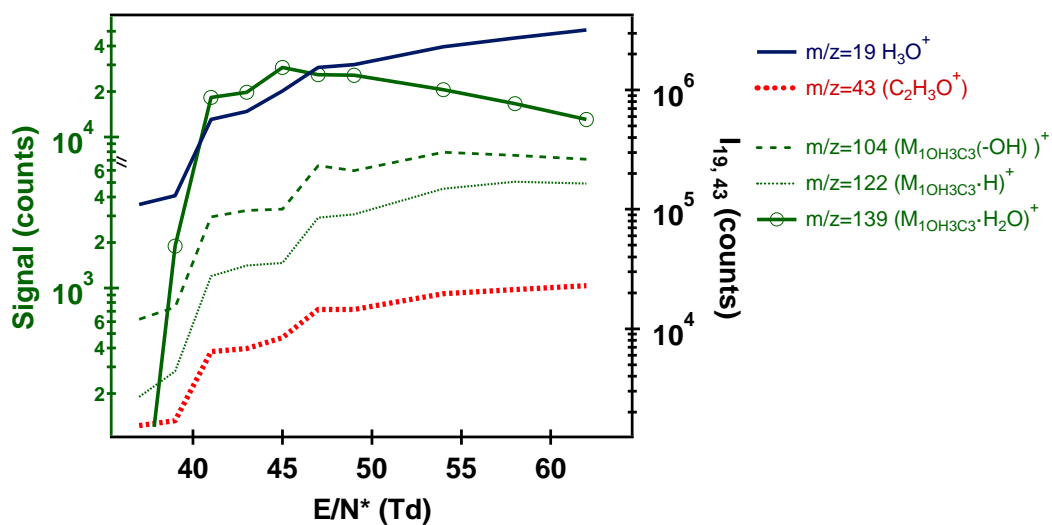
7



1

2 Figure 5. Typical signals due to the 1OH3C3 soft ionization and their behavior as a function  
3 of the E/N ratio variation (left axis) in absence of a RF mode. The fragmentation intensity  
4 depicted by the m/z=43 ion is illustrated together with the H<sub>3</sub>O<sup>+</sup> ion onto the right axis.

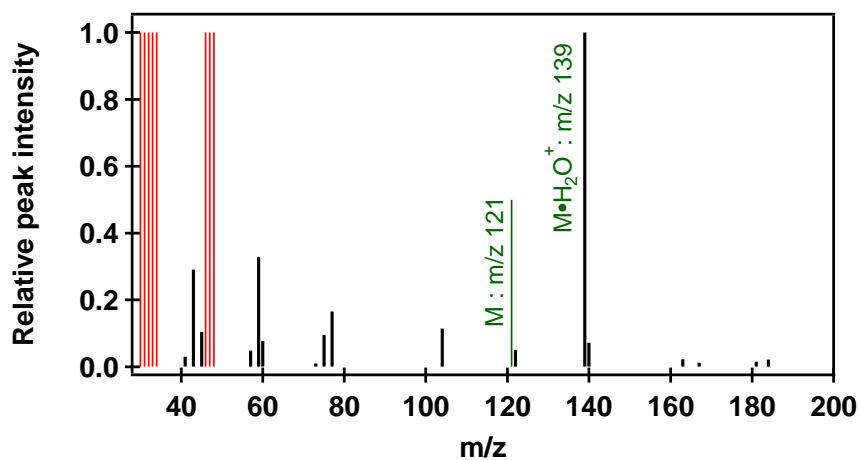
5



1

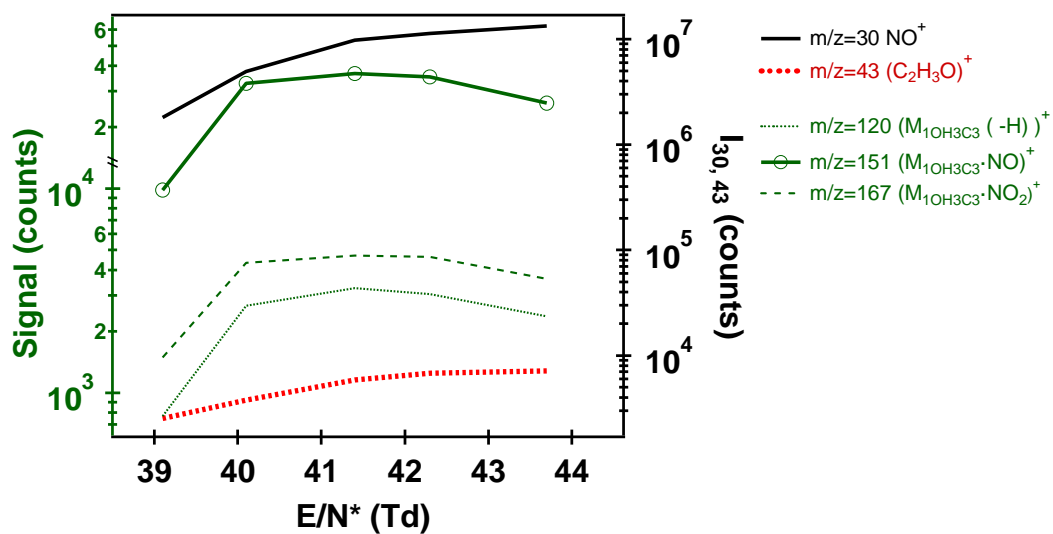
2 Figure 6. Typical signals due to the 1OH3C3 soft ionization and their behavior as a function  
3 of the E/N ratio variation (left axis) in the RF mode. The fragmentation intensity depicted by  
4 the m/z=43 ion is illustrated together with the H<sub>3</sub>O<sup>+</sup> ion onto the right axis.

5



1  
2  
3  
4  
5

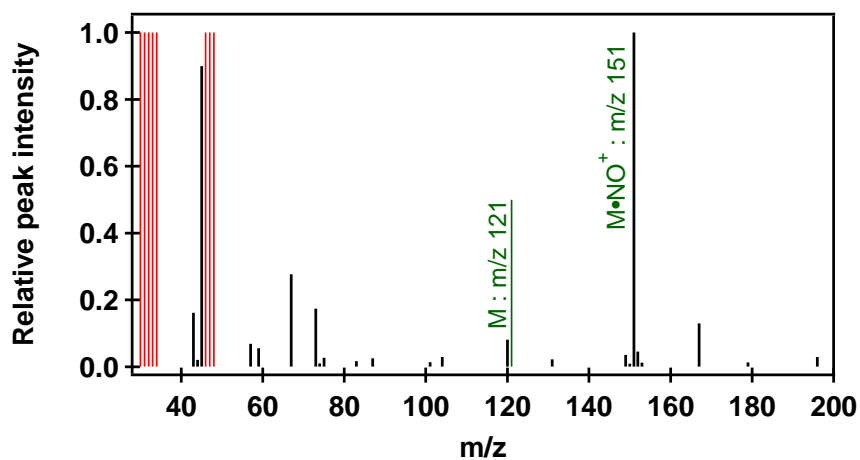
Figure 7. The recorded mass spectrum of 1OH3C3 (black bars) at the lowest extent of fragmentation ( $E/N^* = 45$  Td) in the  $H_3O^+$  ionization mode under the influence of the RF mode.



1

2 Figure 8. The E/N ratio and their influence over the 1OH3C3 ionization and identification  
3 pathways, for several characteristic signals.

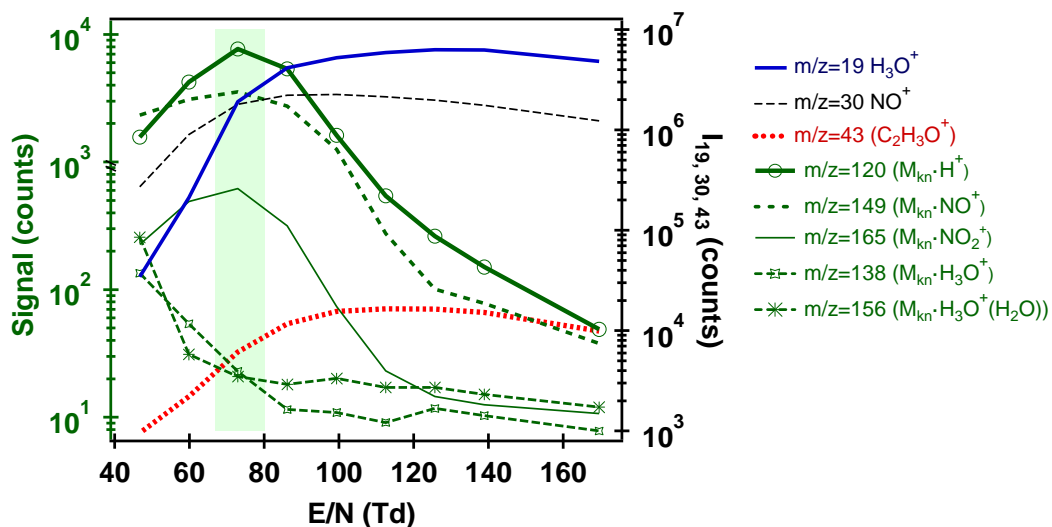
4



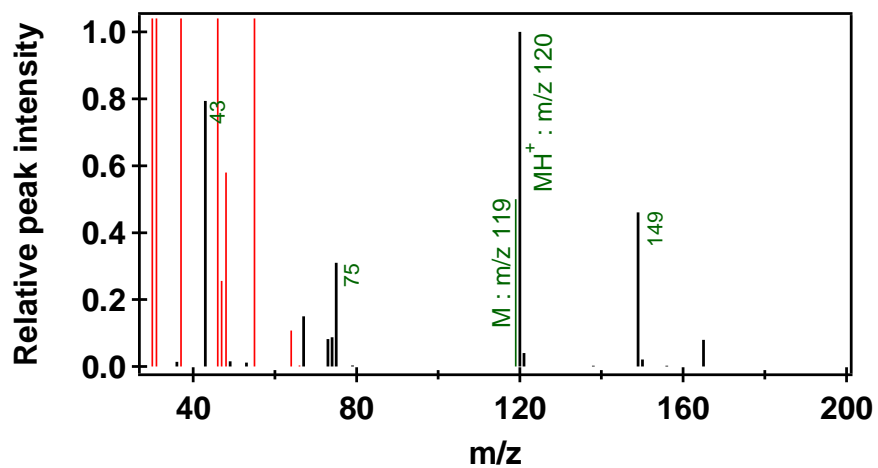
1

2 Figure 9. Recorded mass spectrum of 1OH3C3 (black bars) at the lowest extent of  
3 fragmentation ( $E/N^* = 41$  Td) in  $\text{NO}^+$  ionization mode.

4



1  
2 Figure 10. The KnC3 typical signals distribution over a wide range of E/N ratios (left axis),  
3 illustrating the water cluster ions distribution impact over the keto-nitrates identification. The  
4 fragmentation representative, m/z=43 signal, together with the H<sub>3</sub>O<sup>+</sup> and NO<sup>+</sup> ionizing species  
5 are equally plotted onto the right axis.  
6

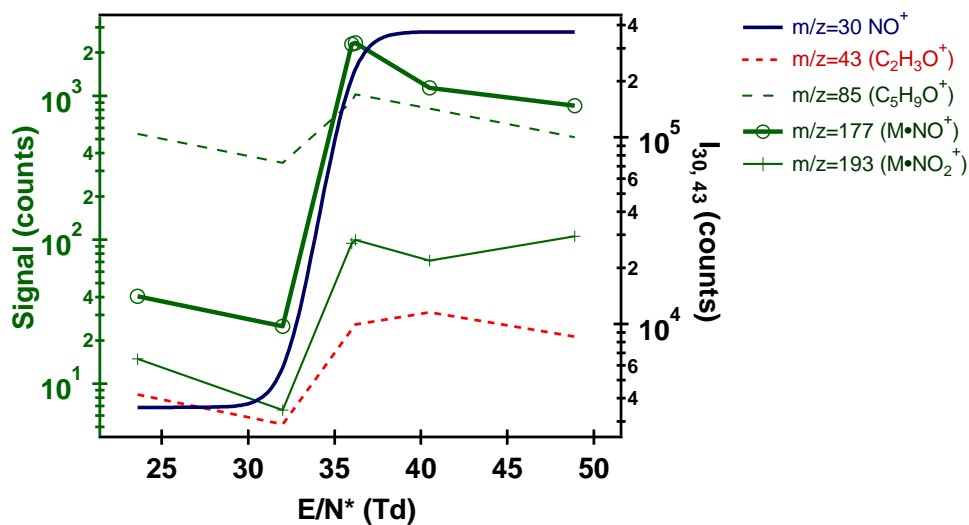


1

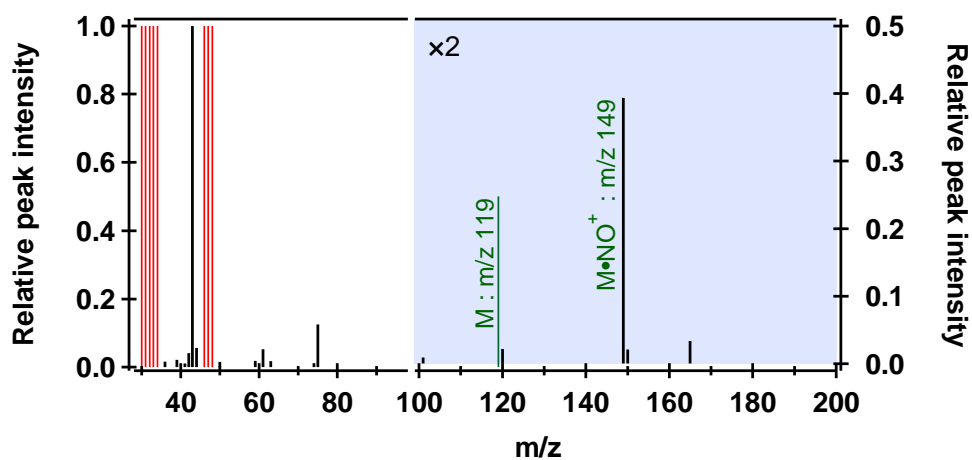
2 Figure 11. Recorded mass spectrum of protonated KnC3 (black bars) for E/N = 75 Td,  
3 corresponding to the highest sensibility for the protonated analyte signal detection (m/z 120).

4





1  
2 Figure 12. The RF mode behavior of typical NO<sup>+</sup> ionization signals of keto-nitrates (KnC5)  
3 under the E/N ratio influence (left axis). Typical distribution of the NO<sup>+</sup> ions and C<sub>2</sub>H<sub>3</sub>O<sup>+</sup>  
4 fragment into the given E/N interval (right axis).  
5



- 1
- 2 Figure 13. Recorded mass spectrum of KnC3 adduct (black bars) at the lowest extent of
- 3 fragmentation ( $E/N^* = 40$  Td) in the  $NO^+$  ionization mode.